LOCKHEED MARTIN ENERGY RESEARCH LIBRARIES

3 4456 0515172 3

ORNL-5414

Experimental Determinations of the Pre-and Postirradiation Thermal Transport and Thermal Expansion Properties of Simulated Fuel Rods for an HTGR

J. P. Moore
T. G. Godfrey
R. S. Graves
W. P. Eatherly
E. L. Long, Jr.
F. J. Weaver

OAK RIDGE NATIONAL LABORATORY
CENTRAL RESEARCH LIBRARY
CIRCULATION SECTION
4500N ROOM 175
LIBRARY LOAN COPY
DO NOT TRANSFER TO ANOTHER PERSON
If you wish someone else to see this report, send in name with report and the library will arrange a loan.
UCN 7969 3 9/77

OAK RIDGE NATIONAL LABORATORY
OPERATED BY UNION CARBIDE CORPORATION · FOR THE DEPARTMENT OF ENERGY

C.77

Printed in the United States of America. Available from
National Technical Information Service
U.S. Department of Commerce
5285 Port Royal Road, Springfield, Virginia 22161
Price: Printed Copy $4.50; Microfiche $3.00

This report was prepared as an account of work sponsored by an agency of the United States Government. Neither the United States Government nor any agency thereof, nor any of their employees, contractors, subcontractors, or their employees, makes any warranty, express or implied, nor assumes any legal liability or responsibility for any third party's use or the results of such use of any information, apparatus, product or process disclosed in this report, nor represents that its use by such third party would not infringe privately owned rights.

ORNL-5414
Distribution Category UC-77

Contract No. W-7405-eng-26

METALS AND CERAMICS DIVISION

HTGR Base-Technology Program
Fueled Graphite Development (189a 01330)

EXPERIMENTAL DETERMINATIONS OF THE PRE- AND POSTIRRADIATION THERMAL TRANSPORT AND THERMAL EXPANSION PROPERTIES OF SIMULATED FUEL RODS FOR AN HTGR

J. P. Moore R. S. Graves E. L. Long, Jr.
T. G. Godfrey W. P. Eatherly F. J. Weaver

Date Published: July 1978

OAK RIDGE NATIONAL LABORATORY
Oak Ridge, Tennessee 37830
operated by
UNION CARBIDE CORPORATION
for the
DEPARTMENT OF ENERGY

LOCKHEED MARTIN ENERGY RESEARCH LIBRARIES

3 4456 0515172 3

CONTENTS

ABSTRACT 1

INTRODUCTION 1

MEASUREMENT TECHNIQUES 4

SPECIMEN DESCRIPTION 4

DESCRIPTION OF CAPSULES 7
- Irradiation History 7
- Capsule Disassembly 7

RESULTS ON UNIRRADIATED SPECIMENS 11
- Coefficient of Thermal Expansion 11
- Electrical Resistivity and Seebeck Coefficient 13
- Thermal Conductivity 13

RESULTS ON IRRADIATED SPECIMENS 17
- Visual 17
- Volume 17
- Coefficient of Thermal Expansion 17
- Electrical Resistivity 17
- Absolute Seebeck Coefficient 20
- Thermal Conductivity 20

DISCUSSION OF RESULTS 22
- Coefficient of Thermal Expansion 22
- Transport Properties 23

CONCLUSIONS 27

RECOMMENDATIONS 28

ACKNOWLEDGMENTS 28

Appendix A. EXPERIMENTAL DATA 29

Appendix B. CALCULATION OF AN EFFECTIVE PARTICLE λ ASSUMING THAT λ_{matrix} BEHAVES AS DOES λ OF THE UNLOADED SPECIMEN 33

Appendix C. COMPARISON OF THE ELECTRICAL RESISTIVITIES OF SLUG-INJECTED RODS CONTAINING FUEL PARTICLES TO RODS CONTAINING SIMULATED PARTICLES AND TO EXTRUDED RODS 35

EXPERIMENTAL DETERMINATIONS OF THE PRE- AND POSTIRRADIATION THERMAL TRANSPORT AND THERMAL EXPANSION PROPERTIES OF SIMULATED FUEL RODS FOR AN HTGR

J. P. Moore, T. G. Godfrey, R. S. Graves, F. J. Weaver, W. P. Eatherly, and E. L. Long, Jr.

ABSTRACT

The thermal conductivity, electrical resistivity, coefficient of thermal expansion, volume, and Seebeck coefficient of simulated fuel rods for a high-temperature gas-cooled reactor (HTGR) were measured before and after neutron irradiations to 13.5×10^{25} neutrons/m^2 at nominal irradiation temperatures of 1220 K. These measurements were made as functions of volume percent particle loading, temperature, and neutron fluence. The thermal conductivities decrease with increasing particle loading at all measurement temperatures. The large difference between the properties of specimens from two fabrication processes (extrusion and slug injection) is attributed to the fact that the densities of the continuous phases within the elements differ by a factor of 2.6. Increases in the thermal conductivity with initial neutron fluence of some of the extruded specimens are attributed to partial ordering of carbonaceous material within the composites, but an unambiguous quantitative analysis is difficult. Some electrical resistivity results obtained on slug-injected unirradiated fuel rods show that the thermal conductivity would probably be affected by graphite shim content. Previous investigators have estimated that the thermal conductivity of slug-injected fuel rods would never go below 6.9 W/m·K, but measurements on a slug-injected specimen with 36.5% simulated fuel and 20.2% shim yielded a value of 5 W/m·K after 8.6×10^{25} neutrons/m^2.

INTRODUCTION

The physical properties of fuel elements are important parameters in controlling fuel lifetime during reactor operation. These properties usually are functions of (1) temperature, (2) neutron flux, (3) neutron fluence, (4) temperature during neutron irradiation, and (5) fuel element fabrication details. The fuel rods for prospective high-temperature gas-cooled reactors (HTGR)[1] are composite materials consisting of spheroidal fuel particles contained in a carbonaceous matrix. In addition, the fuel particles, as shown in Fig. 1, are composites because they consist of fuel particles (UC_2, UC_xO_y, or ThO_2) surrounded by several coatings designed to retain fission products during the particle lifetime. This composite structure leads to properties that are complex functions of time and temperature. Neutron irradiation makes the transport parameters of composites even more complex by having different effects on the individual components such as UO_2 (ref. 2), graphite,[3] and the carbonaceous matrix.[4] During fuel element use, neutron irradiation places a thermal gradient on the fuel element, and fuel kernels may migrate up this gradient causing coated particle failure as soon as the fuel passes through

1. Gas-Cooled Reactor Programs, *High-Temperature Gas-Cooled Reactor Base Technology Program Progr. Rept. July 1, 1975–Dec. 31, 1976*, ORNL-5274 (1978).

2. International Atomic Energy Agency, *Thermal Conductivity of Uranium Dioxide*, report of Panel on Thermal Conductivity of Uranium Dioxide, Vienna, April 26–30, 1965, IAEA TR Series, No. 59.

3. J. P. Moore, R. S. Graves, and D. L. McElroy, *Nucl. Technol.* 22, 88 (1974).

4. W. W. Delle, G. Haag, H. Nickel, H. A. Schulze, and R. E. Schulze, "Influence of the Irradiation Induced Graphitization of Graphitic Materials on Their Property Behavior Under Fast Neutron Exposure at High Temperatures," report JUL-1128-RW, Der Kernforschungsanlage Jülich, Federal Republic of Germany, 1974.

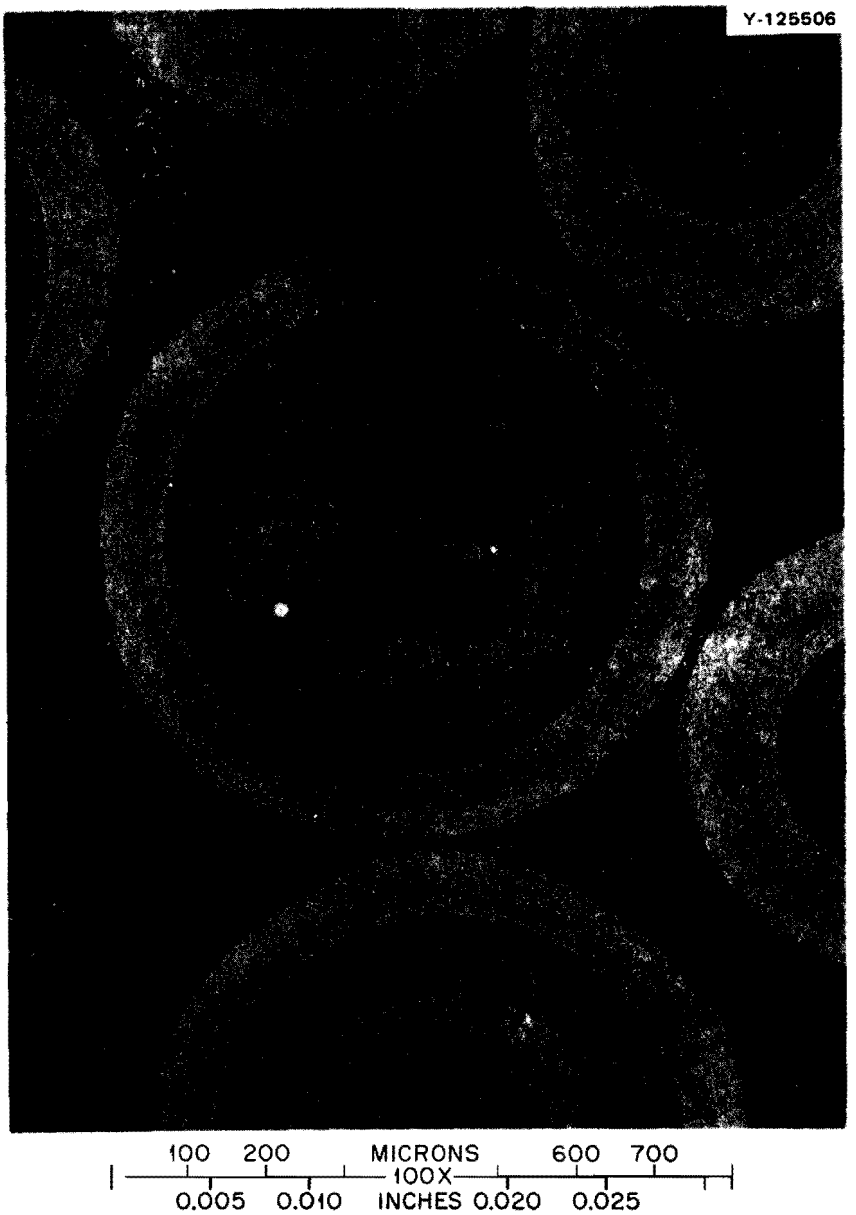

Fig. 1. Photomicrograph of a simulated fuel rod containing 58-vol % particles. The inner particle cores of inert carbon are surrounded by two pyrolytic carbon coatings of different thicknesses.

the particle coatings.[5] A failure of this type is shown in Fig. 2,[5] and the origin of the term *amoeba effect* is readily apparent. This effect is dependent on thermal gradient, temperature, and, therefore, the thermal conductivity of the fuel element.[5-7]

5. R. A. Olstad and E. L. Long, Jr., *An Irradiation Test of Candidate HTGR Recycle Fuels in the H1 and H-2Capsules*, ORNL/TM-4397 (April 1975).

6. R. A. Olstad and E. L. Long, Jr., *An Irradiation Test of Candidate HTGR Recycle Fuels in the H-1 and H-2 Capsules*, ORNL/TM-4397 (April 1975).

7. F. J. Homan and E. L. Long, Jr., *Irradiation Performance of HTGR Recycle Fissile Fuel*, ORNL/TM-5502 (August 1976).

Fig. 2. Kernel migration through its coating and into the adjacent particles after operation near 1623 K with a gradient of about 1.4×10^5 K/m.

There are two primary techniques for fabricating coated particle fuel rods.[8] The first, and traditional, technique involves pouring coated fuel particles into a mold and then injecting a paste containing graphite flake into the voids between particles. Because poured fuel spheres normally consume about 58% of a volume, this technique dictates a volume particle loading of 58%. When lower fuel concentration is required, a certain fraction of the particles will consist of inert "shims" of graphite.

8. R. J. Hamner, J M Robbins, and W. P. Eatherly, "Properties of Extruded Fuel Rods for HTGR Applications," in *Proc. of the 13th Biennial Conference on Carbon, July 18-22, 1977, Irvine, Calif.*

Thus, a fuel loading of 35% would mean 35-vol % fuel particles plus 23-vol % shim particles in the element. This fabrication technique, referred to as slug injection, produces a material of low matrix density.

A second technique for fuel element fabrication is extrusion. Coated fuel particles are mixed in a paste and extruded through a die. This technique has flexibility for varying the particle loading from 0 to nearly 45 vol % and yields a high-density matrix. Particle fracture during extrusion sets the upper loading limit.

The goal of this experiment was the determination of thermal conductivity, λ; electrical resistivity, ρ; coefficient of thermal expansion, CTE; and absolute Seebeck coefficient, S, of simulated fuel elements fabricated by these two techniques. These determinations were made as functions of volume percent particle loading, temperature, and neutron fluence.

MEASUREMENT TECHNIQUES

All λ, ρ, and S values above 390 K were measured in a technique by which heat was constrained to flow along the axis of a specimen in the shape of a right circular cylinder.[9] Radial heat flow was minimized with a guard cylinder, and corrections were made for any small radial flow. For historical reasons this technique is called the high-temperature longitudinal method (HTL) and has uncertainties of ±5%, ±0.8%, and ±0.2 μV/K for the three properties respectively. These errors are larger than normally experienced with this technique because the specimens were abnormally short and because the thermocouples had to be pressed into sensor holes rather than the usual (and more precise) spot welding into place. Figure 3 shows a specimen with part of the guard cylinder removed. A heater, located inside the upper specimen cavity, contained a wire-wound resistor that was used to establish a temperature gradient along the specimen. The temperature on the guard-cylinder heater was automatically controlled to equal the temperature on the specimen heater so that heat exchange between guard cylinder and specimen was minimized. This end was also accomplished by filling the annulus with a fine-grained Al_2O_3 powder, which is not shown in Fig. 3. Some λ measurements were made in a low-temperature system (LTL),[10,11] and these measurements had uncertainties less than 10%.

The CTE measurements were made using a modified technique described by Kollie et al.,[12] and the values have estimated uncertainties of ±4%.

SPECIMEN DESCRIPTION

In actual reactor elements the cores of the coated particles shown in Fig. 1 would be either UC_2, UC_xO_y, or ThO_2. Therefore, neutron irradiation of actual fuel elements would make them extremely

9. J. P. Moore, D. L. McElroy, and R. S. Graves, *A Technique for Determining Thermal and Electrical Conductivity and Absolute Seebeck Coefficient Between 300 and 1000 K,* ORNL-4986 (September 1974).

10. M. J. Laubitz and D. L. McElroy, *Metrologia* 7(1), 1 (1971).

11. T. K. Holder, *Thermal Conductivity, Electrical Resistivity, and Seebeck Coefficient of High Purity Iron and Selected Iron Alloys from 90 K to 400 K,* ORNL/TM-5539 (June 1977).

12. T. G. Kollie, D. L. McElroy, J. T. Hutton, and W. M. Ewing, "A Computer Operated Fused Quartz Differential Dilatometer," p. 129 in *Thermal Expansion—1973,* AIP Conference Proceedings No. 17, American Institute of Physics, New York, 1974.

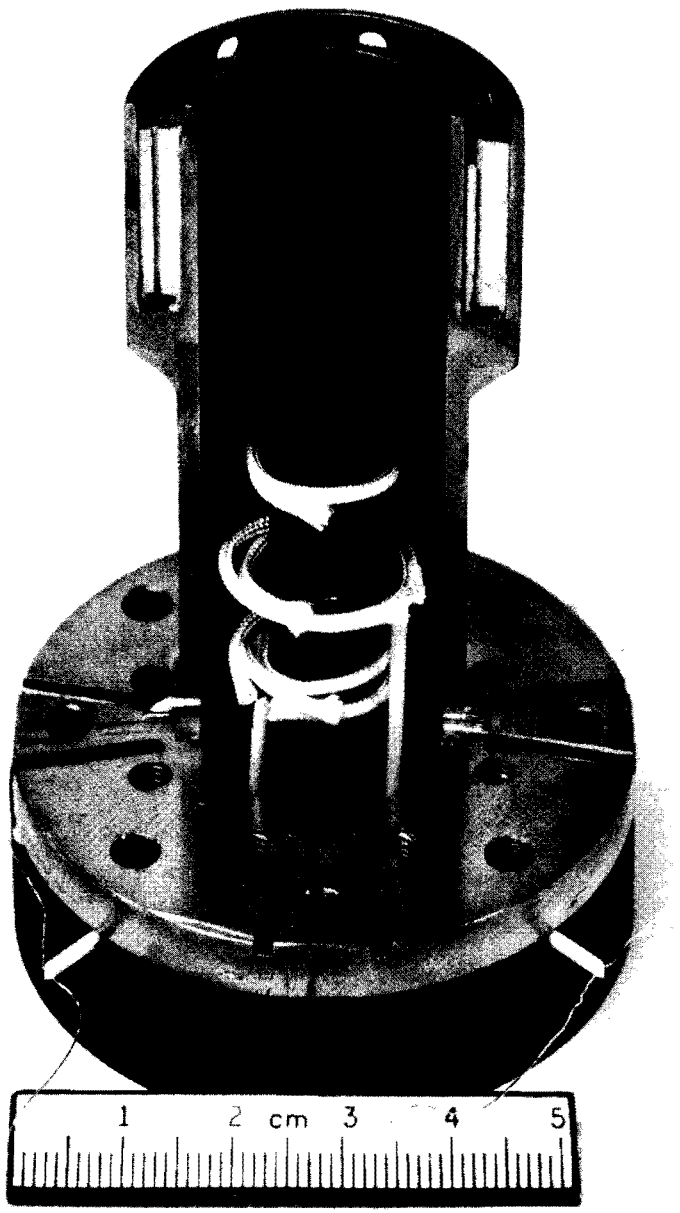

Fig. 3. Photograph of a specimen assembled for measurements of λ, ρ, and S. Part of the primary guard has been removed to show the thermocouple arrangement and heater assembly on the free end of the specimen.

radioactive and prevent postirradiation measurements of the physical properties in our laboratory. For this reason, inert carbon particles with densities of 1.4 Mg/m^3 (and nominal diameters of 470 μm) were used for the particle cores. These carbon kernels were heat treated at 2100 K, and inner and outer pyrolytic carbon coatings with densities of 1 and 2 Mg/m^3 and thicknesses of 73 and 94 μm, respectively, were then applied. These coated particles were heat treated at 2100 K for 600 s prior to bonding into fuel rods.

The matrix of each specimen formed by slug injection consisted of 28.5 wt % graphite filler[13] in pitch.[14] All slug-injected simulated fuel elements were heat treated at 2100 K for 1.8 ks, which yielded a final matrix density of 0.6 Mg/m^3.

Simulated fuel rods with nominal volume percent particle loadings of 0, 13, 22, and 35 were fabricated by the extrusion process. The matrix of each loading was a mixture of 75.7-wt % graphite,[15] 24.3-wt % Thermax,[16] and 25-pph (parts of liquid added per hundred parts of solids being slurried) prepolymerized furfuryl alcohol (Varcum). After heat treating at 2100 K in argon for 1.8 ks, the matrix densities were nominally 1.75, 1.68, 1.63, and 1.62 Mg/m^3 for the extruded specimens with volume percent particle loadings of 0, 13, 22, and 35 respectively. All specimens were right-circular cylinders with nominal OD, ID, and length of 10.16 mm, 3.175 mm and 50.8 mm respectively.

One way to determine the influence of irradiation on a specific property of a material is to measure the property in the unirradiated state, irradiate the same specimen to a known fluence, and then repeat the property measurement. However, as shown in Fig. 3, the λ measurements required attachment of heater and heat sink to opposite ends of the specimen. These protuberances were large enough to prevent placement in a reactor capsule. Therefore, a large number of each specimen type was made, and the five most uniform and homogeneous specimens of each loading were selected for the measurement series on the premise that neutron fluence would have the same effect in all specimens with the same particle loading.

Table 1 presents the electrical resistivity of the 25 specimens selected for this study; these were selected on the basis of their ρ uniformity and the proximity of the ρ to the batch average. The ρ value for each specimen is the average of several measurements made at different positions along the elements. The number in parentheses is the maximum variation of any measured value from the average ρ. The maximum percentage variations for the extruded specimens are 2.7% (22 and 35 vol % unirradiated), whereas the variations for the specimens from the slug-injection process were generally greater with a high of 5.6% for the 57.5-vol % specimen, which was scheduled for four cycles.

13. Grade NF 6353 graphite (natural flake) from Asbury Graphite Mills.
14. Grade 240 petroleum pitch from Ashland Oil, Inc.
15. Grade GLCC-1008 graphite flour from Great Lakes Carbon Corporation.
16. A spherical carbon black from R. T. Vanderbilt Co. Varcum from Reichhold Chemical Corporation.

Table 1. Average electrical resistivities at 300 K (after final machining) of simulated fuel rods in microhm meters

Average loading (%)	Average matrix density (Mg/m^3)	Number of cycles[a]				
		0 (Unirradiated)	1	2	4	6
0[b]	1.75	17.13 (0.19)[c]	17.16 (0.24)	17.12 (0.21)	17.30 (0.12)	17.29 (0.14)
13.2[b]	1.68	22.18 (0.30)	21.89 (0.18)	22.03 (0.28)	21.72 (0.37)	21.71 (0.28)
22.4[b]	1.63	26.55 (0.72)	26.44 (0.23)	26.90 (0.31)	26.40 (0.56)	26.64 (0.38)
34.8[b]	1.62	30.18 (0.81)	30.01 (0.26)	29.56 (0.42)	30.16 (0.41)	30.43 (0.32)
57.5	0.60	78.81 (0.85)	80.80 (1.80)	76.12 (3.60)	81.21 (4.51)	82.25 (3.50)

[a]Each cycle in HFIR roughly equivalent to 2.1×10^{25} neutrons/m^2.
[b]Extruded.
[c]Number in parentheses is maximum deviation from average along the specimen.

The specimens listed under the "0" column of Table 1 were measured in the unirradiated condition. The remaining 20 specimens were irradiated in HFIR[17] for the number of cycles listed. All fluence values given are for $E > 28.8$ fJ. The irradiation temperature for each specimen was a nominal 1220 K. The specimens within a given group (i.e., 1 cycle, 2 cycle, etc.) did not receive the same neutron fluence because of the flux profile within HFIR; the actual fluence value for each specimen is given later in the report in Tables 5, 7, and 8.

DESCRIPTION OF CAPSULES

This experiment initially consisted of four identical capsules designated HT-20, -21, -22 and -23. Each capsule contained five simulated fuel rods. The capsules were designed to operate isothermally at 1220 K and were scheduled to be irradiated in the target region of HFIR for 1, 2, 4, and 6 cycles. A description of the irradiation facility has been reported previously.[18]

The capsule design used to irradiate the simulated fuel rods is shown in Fig. 4. The five simulated fuel rods were placed symmetrically about the horizontal midplane of the HFIR core. The rods were in tandem on a hollow graphite spine with two extruded rods placed above and below a slug-injected rod in each of the capsules. The hollow graphite spines contained tungsten rods that were gamma heat sources for the simulated fuel rods.

In addition to the rods irradiated in capsules HT-20 through -23, four additional rods were irradiated in capsules HT-31 and -32. These additional rods were irradiated to supplement information obtained from HT-20 through -23 and replacements for several rods that were broken during capsule disassembly, as described in the section on postirradiation examination. Capsule HT-31 contained a slug-injected rod (58-vol % particles) and an extruded rod (35-vol % particles); the extruded rod had been irradiated previously in HT-22 for four cycles in position 5. Capsule HT-32 also contained a slug-injected rod (58-vol % particles) and an extruded rod (23-vol % particles); the extruded rod had been irradiated previously in HT-23 for two cycles in position 7. The capsule geometry and temperature for these four replacement rods were the same as for those irradiated in HT-20 through -23. A schematic of capsules HT-31 and HT-32 are shown in Fig. 5.

Irradiation History

The irradiation histories for the target capsules that contained the simulated fuel rods are summarized in Table 2. The calculated thermal and fast fluence values for the fuel rods are listed in Table 3.

Capsule Disassembly

After irradiation, capsules HT-20 through -23 were transferred to the hot cells in Building 3026D for disassembly. Unfortunately, some of the fuel rod specimens were broken during the disassembly operations. The fuel rods had shrunk so much that considerable force was required to remove the graphite spines, which resulted in some damaged or broken specimens.

---

17. High Flux Isotope Reactor, operated at the Oak Ridge National Laboratory.

18. M. J. Kania, *Irradiation Performance of HTGR Fertile Fuel in HFIR Target Capsules HT-12 through -15: Part I—Experiment Description and Fission Product Behavior*, ORNL/TM-5305 (February 1977).

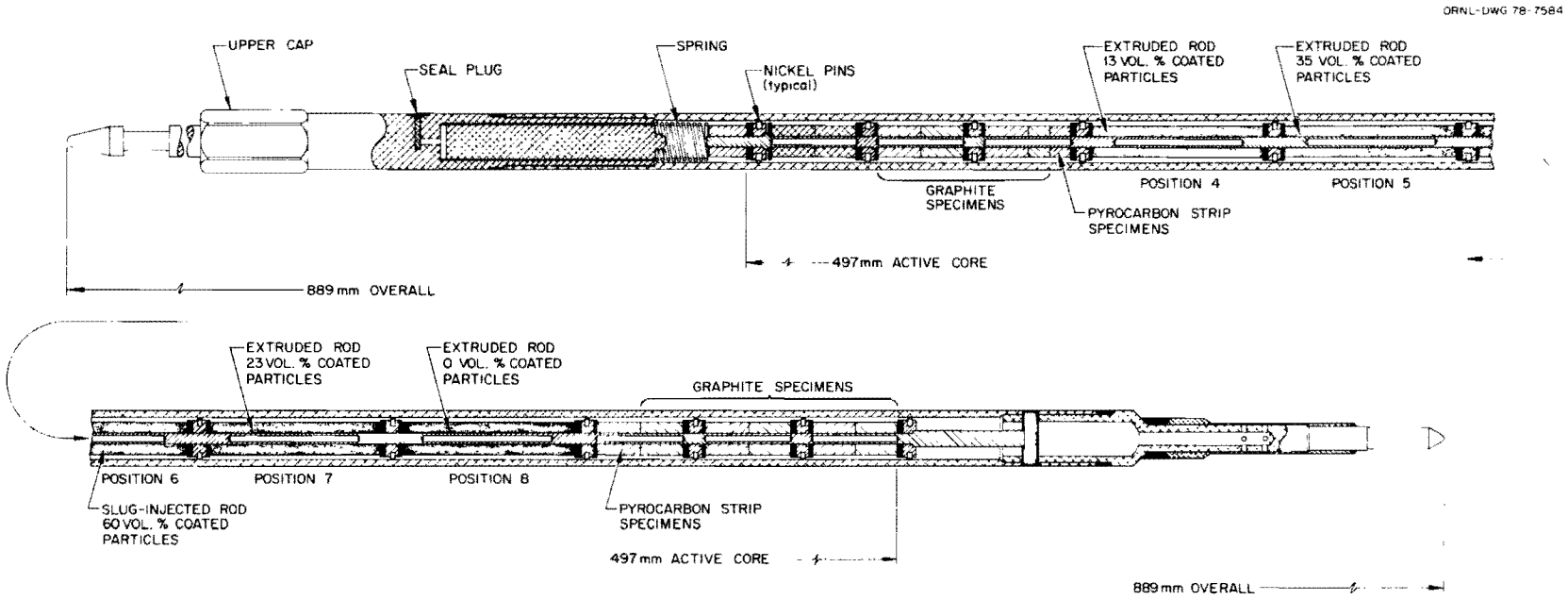

Fig. 4. Target capsule typical of HT-20, -21, -22, and -23 that contained slug-injected and extruded simulated fuel rods for thermal transport and expansion property determinations.

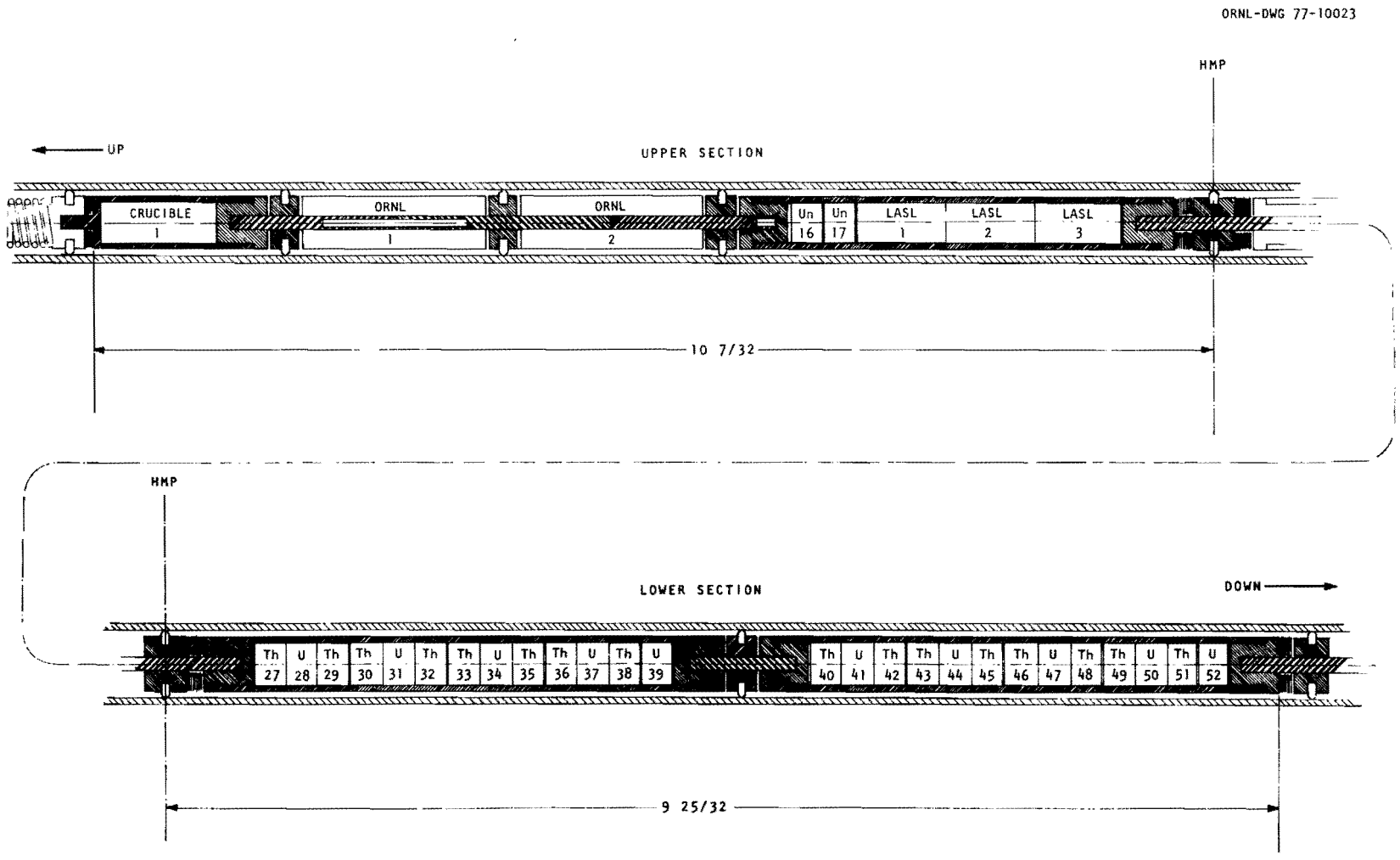

Fig. 5. Schematic diagram of sample placement in HFIR irradiation capsules HT-31 and HT-32. Lengths shown are in inches and correspond to 259.6 and 248.4 mm. Rods ORNL-1 and ORNL-2 are supplemental and replacement rods for HT-20 through HT-23.

Table 2. Operating histories for target capsules that contained simulated fuel rods for thermal transport and expansion property measurements

Target capsule	Facility	HFIR fuel cycle	Begin		End		Irradiation (hr)[a]	
			Time	Date	Time	Date	During cycle	Accumulated
HT-20	F-7	108	1406	6/28/74	1340	7/21/74	551.52	551.52
HT-21	E-2	109	1842	7/22/74	0400	8/15/74	546.88	546.88
		110	1707	8/15/74	2012	9/9/74	549.60	1096.48
		111	1030	9/12/74	0736	10/5/74	548.88	1645.36
		112	0525	10/6/74	0218	10/31/74	547.20	2192.56
		113	0318	11/1/74	1024	11/24/74	558.70	2751.26
		114	1332	11/25/74	0400	12/18/74	54.70	3292.96
HT-22	F-7	109	1842	7/22/74	0400	8/15/74	546.88	546.88
		110	1707	8/15/74	2012	9/9/74	549.60	1096.48
		111	1030	9/12/74	0736	10/5/74	548.88	1645.36
		112	0525	10/6/74	0218	10/31/74	547.20	2192.56
HT-23	A-3	111	1030	9/12/74	0736	10/5/74	548.88	548.88
		112	0525	10/6/74	0218	10/31/74	547.20	1096.08
HT-31	G-5	130	1732	3/14/76	2354	4/6/76	557.76	557.76
		131	2124	4/7/76	2312	4/30/76	552.48	1110.24
		132	2142	5/1/76	0800	5/22/76	489.60	1599.84
		133	2211	5/23/76	1240	6/16/76	546.72	2146.56
HT-32	G-5	140	1900	11/15/76	0400	12/14/76	577.00	577.00
		141	1711	12/15/76	0115	1/10/77	568.07	1145.07
		142	2030	1/10/77	2000	2/3/77	576.50	1721.57
		143	1830	2/5/77	2000	3/1/77	587.50	2309.07

[a]Irradiation time is given in equivalent hours at 100 MW.

Table 3. Fast and thermal fluences for simulated fuel rods irradiated in the target region of HFIR

Specimen	Distance[a] (mm)	Thermal[b] and fast[c] fluence (neutrons/m^2)											
		HT-20		HT-21		HT-22		HT-23		HT-31		HT-32	
		Thermal	Fast	Thermal	Fast	Thermal	Fast	Thermal	Fast	Thermal	Fast	Thermal	Fast
4, 8	114.3	4.63	2.03	2.76	12.09	1.84	8.05	9.19	4.03				
5, 7	57.2	5.28	2.26	3.15	13.51	2.10	9.00	10.50	4.50				
6[f]	0	5.62	2.34	3.35	13.98	2.23	9.31	11.17	4.66				
ORNL-1[f]	196.9									1.36	5.66		
ORNL-2[d]	139.7									3.76[d]	16.30[d]		
ORNL-1[f]	196.9											1.46	6.09
ORNL-2[e]	139.7											12.29[e]	12.39[e]

[a]Distance from horizontal midplane of HFIR core.
[b]$E < 6.6 \times 10^{-20}$ J (0.414 eV).
[c]$E > 28.8$ fJ (0.18 Mev).
[d]Previously irradiated in HT-22, position 5; sum of fluences for HT-22 and HT-31.
[e]Previously irradiated in HT-23, position 7; sum of fluences for HT-23 and HT-32.
[f]Slug-injected fuel rod; all others are extruded rods.

The retrieval of the supplementary and replacement rods from HT-31 and HT-32 was not much better; two rods were recovered intact, and both slug-injected rods were broken. The condition of all of the rods from the five HT-capsules are listed in Table 4. After a period of about one month after removal from HFIR, the activity of most of the simulated fuel rods was low enough to permit removal from the hot cells for the experimental determinations of the thermal transport and expansion properties. The extruded specimen from HT-32 was too hot to permit measurement outside a controlled zone.

Table 4. Condition of fuel rod specimens after removal from capsules HT-20, -21, -22, -23, -31, and -32

No. of HFIR cycles	Capsule	Nominal particle loading (vol %)				
		0	13	23	35	58
1	HT-20	OK	OK	OK	OK	Broken[a]
2	HT-23	OK	OK	OK	OK	Broken
4	HT-22	OK	OK	OK	OK	Broken
6	HT-21	OK	OK	Broken	Broken	Broken
4	HT-31[b]				OK[c]	Broken
4	HT-32[b]			OK[d]		Broken

[a]Some data obtainable since fuel rod was broken in two pieces.

[b]One of the purposes of HT-31 and HT-32 was to provide irradiated slug-injected specimens, but these specimens were broken either during irradiation or capsule disassembly.

[c]Same rod previously irradiated in HT-22, position 5.

[d]Same rod previously irradiated in HT-23, position 7. Specimen too radioactive for measurement after irradiation.

RESULTS ON UNIRRADIATED SPECIMENS

Coefficient of Thermal Expansion

Figure 6 shows that the CTE of each unirradiated bonded-bed fuel rod increased smoothly with increasing temperature. Each curve was fitted with a second-degree polynomial with the coefficients given in Table 5. Figure 7 shows that the CTE at 298 and 973 K increased linearly with particle loading for the unirradiated materials. This indicates that a simple mixing law describes the effect of coated particles on the CTE of a fuel rod. The fact that the slug-injected 58-vol % sample showed a CTE in accord with those of the extruded samples might be considered surprising in view of its low matrix density and different matrix composition. Because porosity variation alone will not change the CTE, the large density differences between the slug-injected and extruded materials had no effect on the CTE. The degree of graphitization does, however, influence CTE; after fabrication heat treatment, the ratios of graphitic carbon to nongraphitic carbon for the extruded matrix and for the injected matrix were about 2 and 1.5 respectively. The matrices were, therefore, actually quite similar. However, because the particles in the specimen with 58-vol % loading were in a closely packed array, the observed thermal expansion was essentially that of the particles and was only slightly affected by the matrix. Therefore, a significant conclusion drawn from the 58-vol % sample data is that the apparent room temperature CTE of these coated particles was less than $4 \times 10^{-6} \cdot K^{-1}$.

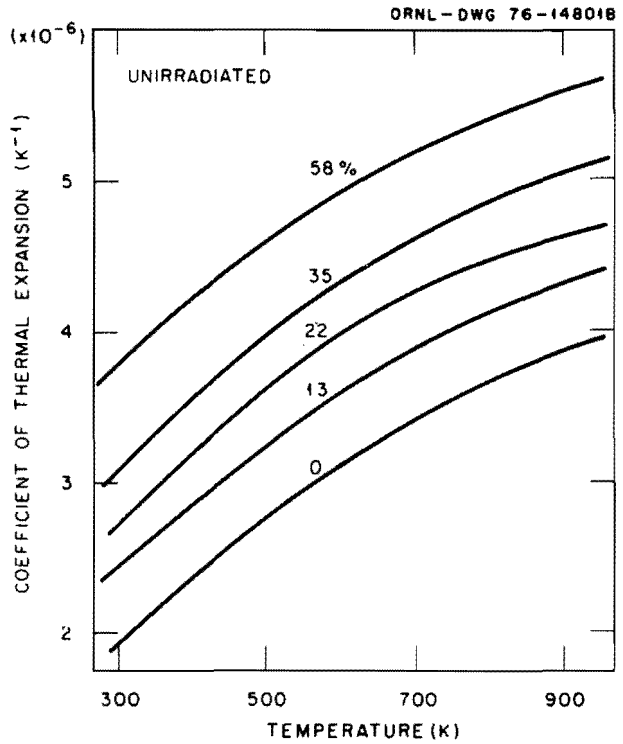

Fig. 6. The CTE of unirradiated simulated fuel rods as functions of temperature.

Table 5. Coefficient of thermal expansion (CTE) of simulated fuel rods

Particle loadings (vol %)	Neutron fluence ($\times 10^{25}$ neutrons/m^2)	CTE (K^{-1}) $\times 10^6 = A + BT + CT^2$			CTE ($\times 10^{-6} \cdot K^{-1}$)	
		A	B	$C \times 10^6$	298 K	973 K
0	0	0.272	0.00628	−2.58	1.92	3.95
0	2.02	−0.012	0.00545	−1.41	1.48	3.95
0	4.03	0.029	0.00502	−0.78	1.45	4.17
0	8.05	−0.545	0.00790	−3.36	1.51	3.96
0	12.1	−0.221	0.00744	−3.31	1.70	3.88
13	0	0.746	0.00627	−2.59	2.38	4.39
13	2.02	−0.152	0.00670	−2.46	1.63	4.04
13	4.03	0.076	0.00502	−0.96	1.49	4.00
13	8.05	−0.549	0.00736	−2.97	1.38	3.80
13	12.1	−0.573	0.00763	−3.43	1.40	3.60
22	0	0.761	0.00736	−3.41	2.66	4.69
22	2.26	0.451	0.00496	−1.34	1.81	4.01
22	4.5	−0.387	0.00675	−2.60	1.39	3.72
22	9.0	−0.687	0.00704	−2.70	1.17	3.60
35	0	1.188	0.00708	−3.11	3.02	5.13
35	2.26	0.155	0.00650	−2.66	1.86	3.96
35	4.5	0.145	0.00469	−0.96	1.46	3.81
58	0	2.038	0.00657	−2.94	3.74	5.66

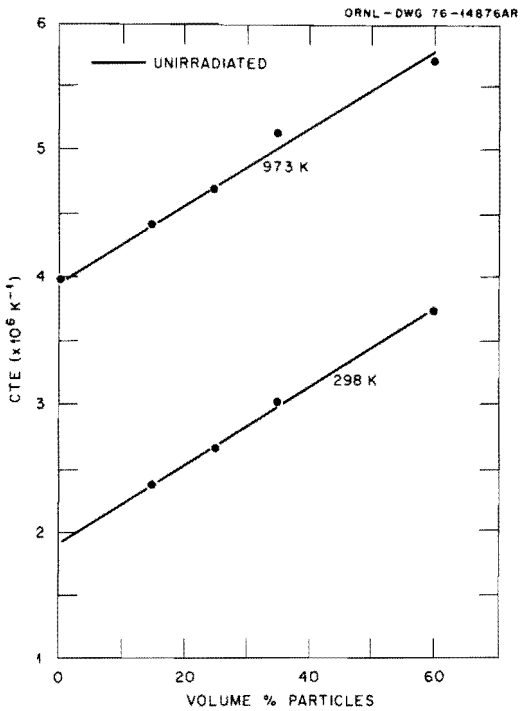

Fig. 7. The CTE vs volume percent particle loading at 298 and 973 K showing the uniform increase with particle loading.

Electrical Resistivity and Seebeck Coefficient

Figure 8 shows the ρ and S of all unirradiated materials as functions of temperature. Electrical resistivity of irradiated and unirradiated materials are given in Table 6, and smoothed ρ values are given in Table 7. The ρ of each specimen decreased smoothly with increasing temperature in a manner similar to isotropic graphites. At a constant temperature, the ρ increased smoothly with increasing particle loading for the extruded material, but the ρ of the slug-injected specimen with 58% loading was much higher than that of the extruded specimens. This was partially due to the lower density matrix of the slug-injected specimen.

Thermal Conductivity

The λ results from measurements on unirradiated simulated fuel elements are shown in Fig. 9 as a function of temperature, and smoothed values are given in Table 8. The matrix material of the extruded specimens had the highest λ. The addition of particles lowered λ at all temperatures; this is illustrated in Fig. 10 for T = 400 K. This smooth decrease of λ with increasing particle loading is similar to the decrease in electrical conductivity, $\sigma = \rho^{-1}$, which is also shown. Figure 9 also shows data obtained by Johnson[19] on two slug-injected specimens. One of these had 58-vol % fuel particles and the other had 35-vol % fuel particles with 22-vol % shim. Johnson's data are in general agreement with the extrapolation of the present results on an unirradiated slug-injected specimen.

19. W. R. Johnson, *Thermal Conductivity of Large HTGR Fuel Rods*, GA-A12910 (GA-LTR-9) (March 1974).

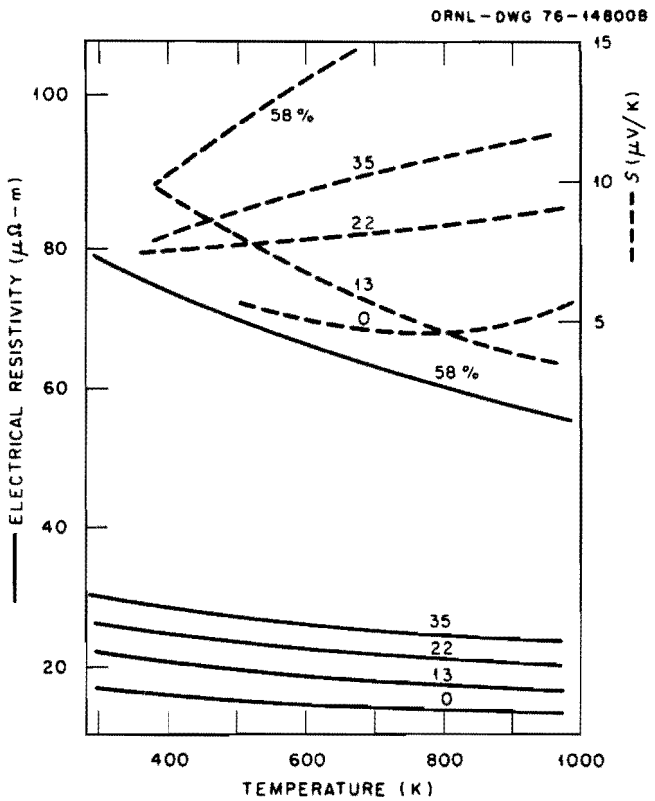

Fig. 8. The ρ and S of unirradiated specimens vs temperature.

Table 6. Electrical resistivity at 300 K of simulated fuel rods before and after irradiation in HFIR in microhm meters

Particle loading (vol %)	Number of cycles[a]				
	0	1	2	4	6
0	17.20	26.82	28.81	39.25	67.21
13	21.90	32.31	34.58	43.74	67.04
22	26.59	37.14	39.61	51.08	90.76
35	30.07	38.75	40.15	51.24	*b*
58	79.11	95.50	*b*	*b*	*b*

[a]Each cycle in HFIR equivalent to between 2.0×10^{25} to 2.34×10^{25} neutrons/m^2 depending on position. Exact values are given in Appendix A.

[b]Broken during irradiation or during capsule disassembly.

Table 7. Smoothed values of the electrical resistivity of simulated fuel rods in microhm meters

Particle loading (vol %)	Neutron fluence ($\times 10^{-25}$ neutrons/m^2)	Temperature (K)							
		300	400	500	600	700	800	900	1000
0	0	17.0	16.0	15.2	14.5	14.0	13.6	13.4	13.3
0	2.02	26.6	24.1	22.0	20.2	18.6	17.4	16.5	15.9
0	4.03	28.8	29.0	27.4	24.1	22.4	20.8	19.2	17.6
0	8.05	39.2	36.2	33.4	31.0	29.0	27.2	25.6	24.2
0	12.09	67.2	63.0	59.6	56.2	53.0	50.1	47.4	45.0
13	0	22.2							
13	2.02	32.1	29.2	26.7	24.5	22.7	21.2	20.1	19.3
13	4.03	34.6	31.4	28.7	26.4	24.6	23.1	22.0	
13	8.05	43.7	40.3	37.4	34.8	32.4	30.2	28.5	26.9
13	12.09	67.0	61.6	57.0	52.8	49.2	46.0	43.0	40.4
22	0	26.3	25.0	23.8	22.8	21.9	21.2	20.7	20.3
22	2.26	36.9	33.4	30.4	28.0	26.0	24.2	22.9	21.8
22	4.50	39.6	35.8	32.6	29.8	27.5	25.6	23.8	22.5
22	9.0	51.1	46.7	43.0	39.8	36.9	34.3	32.0	29.8
22	13.5	90.8							
35	0	30.0	28.5	27.1	25.9	25.0	24.3	23.7	23.4
35	2.26	38.7							
35	4.50	40.1	36.6	33.6	30.8	28.4	26.3	24.6	23.5
35	9.0	51.2	46.3	42.4	39.3	36.6	34.0	33.4	32.7
35	13.5								
58	0.0	78.5	74.1	70.1		63.1	60.1	57.5	55.3

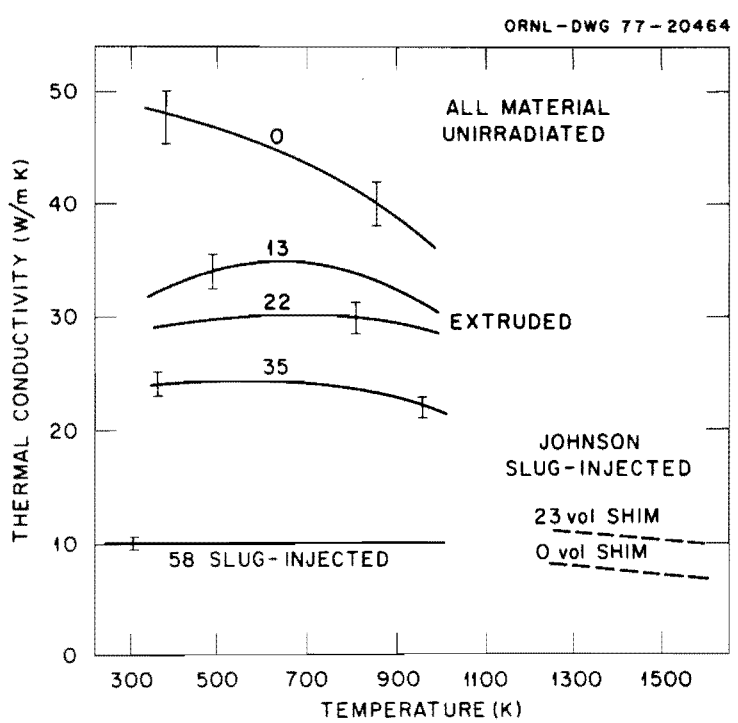

Fig. 9. The λ of unirradiated simulated fuel rods vs temperature for five loadings. High-temperature data from Johnson[19] are shown for comparison.

Table 8. Smoothed values for the thermal conductivity of simulated fuel rods with nominal particle loadings of 0, 13, 22, 35, and 58 vol %

Particle loadings (vol %)	Neutron fluence ($\times 10^{-25}$ neutrons/m^2)	Thermal conductivity (W/m·K)						
		400	500	600	700	800	900	1000
0	0	47.5	47.2	46.2	44.6	42.1	39.0	35.3
0	2.02	40.4	42.3	43.3	43.3	42.4	40.6	38.0
0	4.03	38.6	39.2	39.1	38.4	37.0	35.3	
0	8.05	19.9	21.2	21.9	22.0	21.7	20.9	20.0
0	12.09	9.6	10.1	10.5	10.6	10.6	10.6	10.5
13	0	33.0	34.6	35.2	34.9	34.0	32.2	30.6
13	2.02	32.8	34.1	34.5	34.2	33.6	32.3	30.4
13	4.03	29.2	29.7	29.9	29.7	29.3	28.8	28.0
13	8.05	18.8	19.8	20.5	21.0	21.0	20.6	19.7
13	12.09	11.2	12.0	12.5	12.7	12.5	12.0	11.0
22	0.0	29.5	30.0	30.2	30.4	30.2	29.6	29.2
22	2.26	28.6	30.0	30.8	30.5	29.6	28.1	26.0
22	4.50	28.1	28.7	28.8	28.6	28.0	27.1	26.0
22	9.0	18.0	18.8	19.2	19.2	18.9	18.3	17.6
22	13.5							
35	0	24.2	24.6	24.7	24.2	23.3	22.0	
35	2.26	27.6	29.0	30.0	30.2	29.6	28.0	26.0
35	4.50	22.2	24.0	25.6	26.7	27.8	28.5	28.5
35	9.0	12.5	13.4	14.2	14.4	14.0	13.0	11.5
35	13.5							
58	0	10.2	10.8	11.2	11.3	11.2	10.8	10.4
58	2.34	11.8	12.					
58[a]	8.6	5	5					
35[b]	0	39.3	37.4	35.3				

[a]Archive specimen with 20.2% shim and simulated fuel particles similar to those used throughout this report. The matrix of this specimen was fabricated from the same material as the other slug-injected samples.

[b]Unirradiated specimen that has been graphitized at 2900 K.

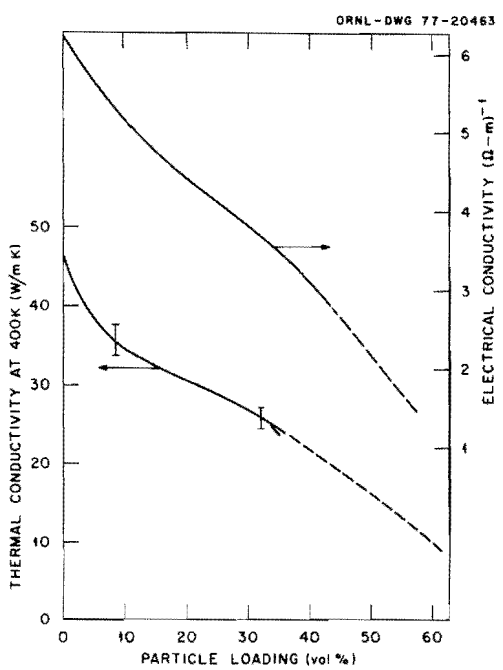

Fig. 10. Thermal (at 400 K) and electrical (at 300 K) conductivities of unirradiated simulated fuel rods showing the smooth decrease with particle loading and the similar behavior of σ and λ.

RESULTS ON IRRADIATED SPECIMENS

Visual

With one exception, all extruded specimens in this test survived neutron irradiation. The one exception was the specimen with 35-vol % particles which had gone to 13.5×10^{25} neutrons/m^2 ($E > 28.8$ fJ) or 6 cycles in HFIR.

In contrast, all slug-injected specimens were very fragile and fell apart either during irradiation or during careful routine handling. This is similar to the behavior observed by others[20] on slug-injected specimens with varying shim content.

Volume

The properties of the simulated fuel rods studied in this experiment changed significantly with neutron irradiation. The volumetric changes as a function of neutron fluence are shown in Fig. 11. All specimens showed an initial decrease in volume with increasing fluence up to about 4×10^{25} neutrons/m^2. Above that fluence, this trend reversed, and they reached their initial volume between 9×10^{25} and 12×10^{25} neutrons/m^2.

Coefficient of Thermal Expansion

Low-order polynomials which express the CTE results obtained on the simulated fuel rods are given in Table 5. In addition, values for CTE at 298 and 973 K are tabulated. As was shown in Fig. 7 for the unirradiated samples, the CTEs at 298 and 973 K were almost directly proportional to the particle content. However, this behavior changed after the initial irradiation cycle ($\sim 2 \times 10^{25}$ neutrons/m^2), and the CTE became almost independent of particle loading for all extruded specimens as shown in Fig. 12. Although the broken slug-injected specimen containing 58-vol % particles was satisfactory for some limited λ measurements, it was too short for CTE determinations, and no CTE data were obtained on the 58-vol % loading series after irradiation.

Electrical Resistivity

The ρ of all specimens was measured at room temperature following irradiation, and the results are given in Table 6 and plotted in Fig. 13. All extruded materials behaved similarly. The electrical resistivity of each increased initially with neutron fluence, reached a momentary plateau between 3×10^{25} and 4×10^{25} neutrons/m^2, and then began another rapid increase with fluence. The positive deviations of ρ above the relatively flat regions near 4×10^{25} neutrons/m^2 coincided with the minima in the $\Delta V/V_0$ curves of Fig. 9. The ρ of the 58-vol % loaded specimen from the slug-injection process increased uniformly with fluence and did not have a short-term flat region similar to the one noted in the extruded specimens. The ρ (300 K) of the specimens with 22- and 35-vol % particles and the ρ (300 K) of the 0- and 13-vol % particles tended to merge at higher fluence. This rather interesting effect is apparent in Fig. 14, which shows ρ (300 K) versus particle loading after each reactor cycle. The 22- and 35-vol % specimens had essentially the same ρ after two cycles in HFIR whereas the 0- and 13-vol % specimens had the same ρ after six cycles. Measured values of ρ are given in Appendix A, and smoothed ρ data for all specimens are given in Table 4.

---

20. W. R. Johnson, R. L. Hamner, J M Robbins, and B. H. Montgomery, *Postirradiation Examination of Capsules HT-24 and HT-25,* GA-A13486 (September 1975).

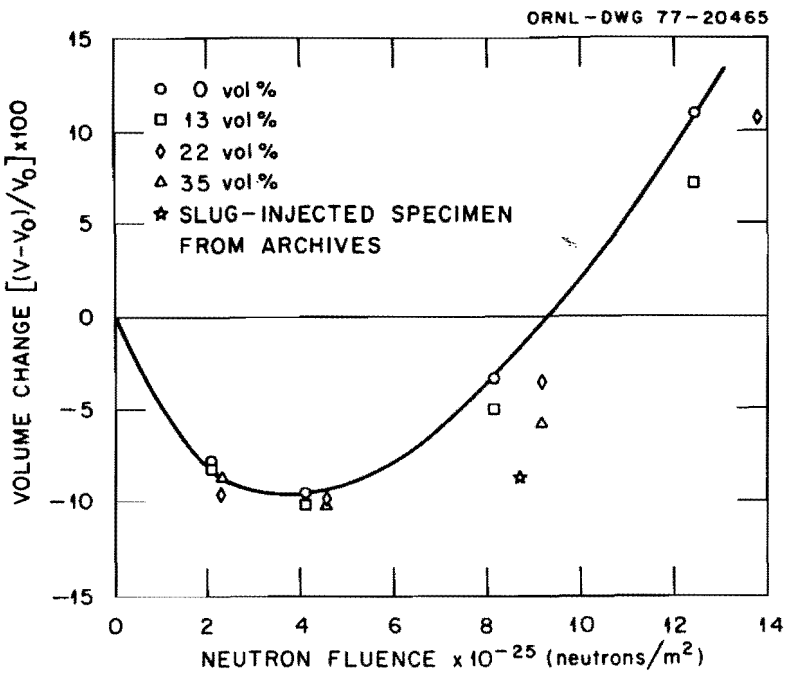

Fig. 11. Specimen volume change (at room temperature) vs fluence showing a minimum volume occurring near 4×10^{25} neutrons/m^2. The slug-injected material has the greatest change with fluence, and no material returns to its original size before 9×10^{25} neutrons/m^2.

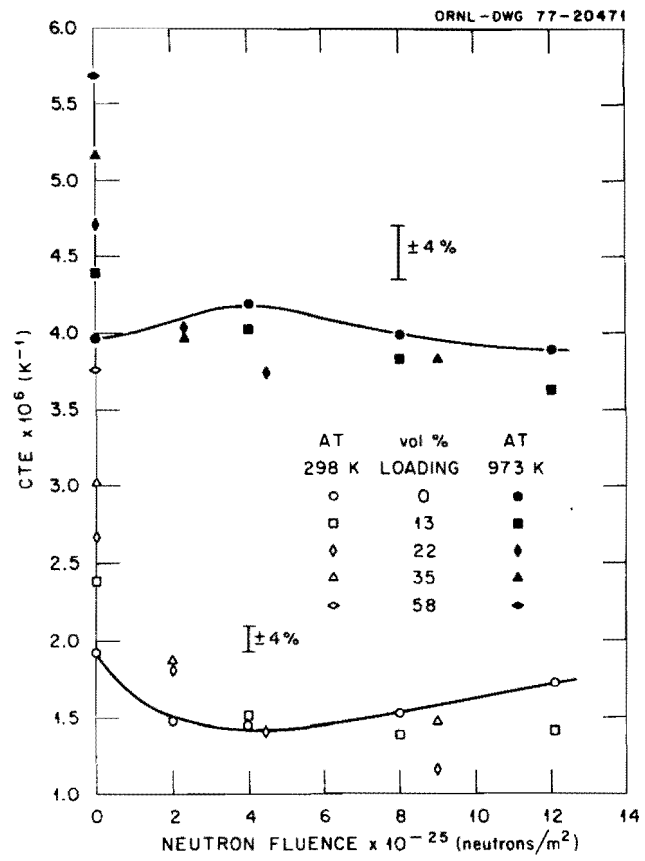

Fig. 12. The CTE of extruded and slug-injected specimens vs fluence showing the relative insensitivity to particle loading and neutron fluence after one cycle. Solid lines connect data for the rod that contained 0-vol % particles.

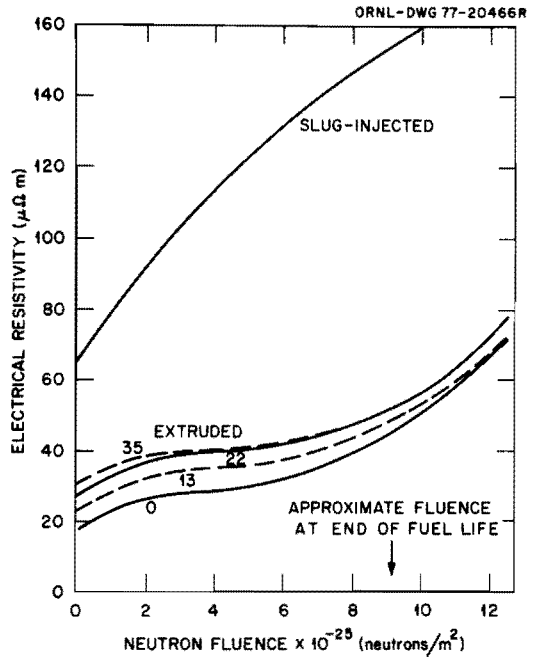

Fig. 13. The electrical resistivity at room temperature vs neutron fluence for the simulated fuel rods showing the plateau region observed in the extruded specimens.

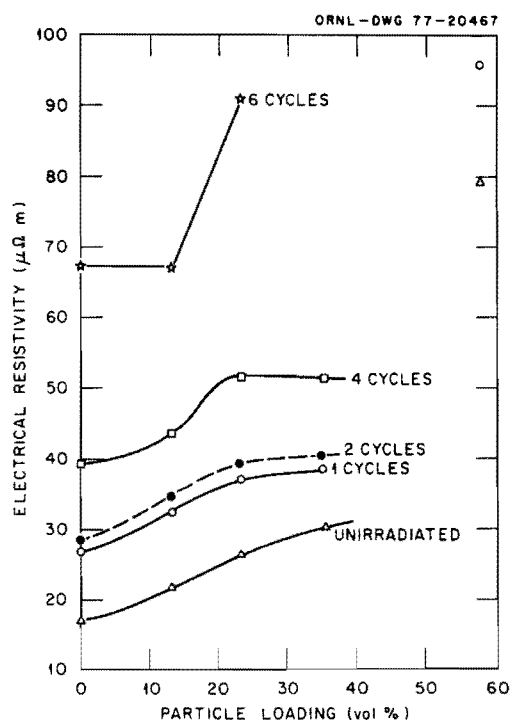

Fig. 14. The ρ of simulated fuel rods for various reactor cycles vs particle loading.

Absolute Seebeck Coefficient

All Seebeck coefficient data are given in Appendix A. With the exception of the unirradiated specimen with 13-vol % particles, the S for a specific particle loading did not vary greatly with temperature. Therefore, Fig. 15 shows the S data obtained at the lowest measurement temperature (~390 K) versus neutron fluence. All loadings had positive values for S, which increased in magnitude with increasing fluence and then began decreasing at roughly the same fluence at which $\Delta V/V_0$ minimized and ρ plateaued.

Thermal Conductivity

All thermal conductivity results on the irradiated specimens are given in Appendix A, and smoothed values are presented in Table 8. The initial effects of neutron irradiation after one reactor cycle are shown in Fig. 16. The specimen fabricated using the slug-injection process still had the lowest λ, but it is about 10% higher than data obtained on the unirradiated specimen. The data for this specimen were limited in temperature range because the broken specimen was so short that measurements were restricted to the LTL, which has an upper limit of 400 K.

The λ of the extruded specimen with 35-vol % particles actually increased during the first irradiation cycle. This unexpected result was verified by obtaining data on the same specimen using the LTL. Results from the two techniques agreed to within ±3%. The λ of the 22- and 35-vol % specimens were nearly equivalent after one reactor cycle. This is reminiscent of the similar ρ values of the two loadings after one cycle. The λ of the 13-vol % and the 22-vol % specimens was almost unaffected by the first 2×10^{25} neutrons/m^2 whereas the matrix material λ (0 vol %) dropped by about 15%.

Although the λ curves varied somewhat with temperature, the results at 400 K are representative, and these were selected to compare the results at higher fluence.* The smoothed values at 400 K from Table 8 are, therefore, shown in Fig. 17 versus fluence. The specimen labeled "58 vol %–20.2% Shim" was not an original part of this test but was obtained from a previous irradiation experiment. This specimen was listed as #14-4 in Table #4 of Johnson et al.[20] One conclusion of Johnson et al.[20] is that this specimen contained the superior shim type of the many that they tested. The matrix material of the extruded specimen (0 vol %) had the highest λ initially. This λ decreased but had a plateau over a limited fluence range. This behavior is similar to that observed by Delle et al.[4] on other carbonaceous materials. The λ of the 13- and 22-vol % specimens remained essentially constant initially and then decreased smoothly with increasing fluence. The extruded specimen with 35-vol % loading and the slug-injection specimen with 58-vol % loading had λ that increased with fluence initially and then decreased beyond 3×10^{25} or 4×10^{25} neutrons/m^2. The reason for this behavior is discussed in a later section.

The λ value of 5 W/m·K at 8.6×10^{25} neutrons/m^2 was obtained on a slug-injected fuel rod with a total particle loading near 58 vol %. Part of this, however, was graphite shim so that the simulated fuel particles consumed only 36.5 vol %. Therefore, this datum can be compared to the extruded specimen with 35-vol % particles. This comparison at 8.6×10^{25} neutrons/m^2 showed that the ratio of λ from the extruded material to λ from the slug-injection material was 2.6.

*This also permitted use of the two data sets generated in the LTL, which has an upper temperature near 400 K.

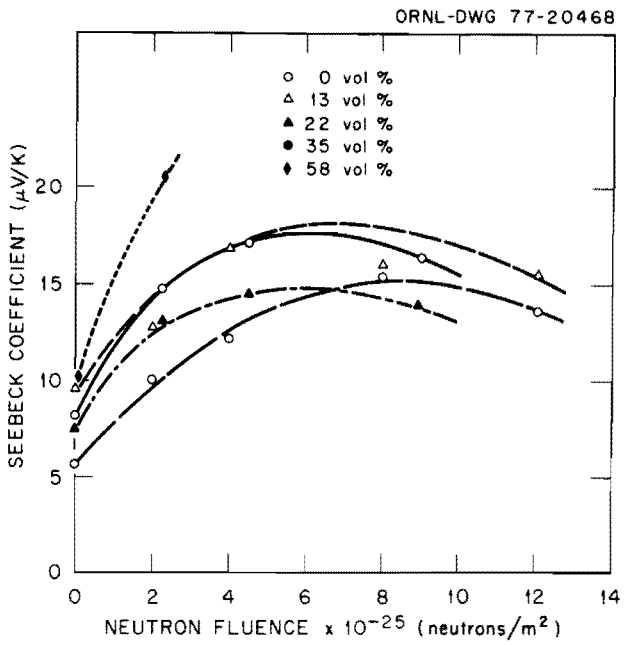

Fig. 15. Absolute S of simulated fuel rods near 390 K vs neutron fluence showing the maximum that occurs for each particle loading.

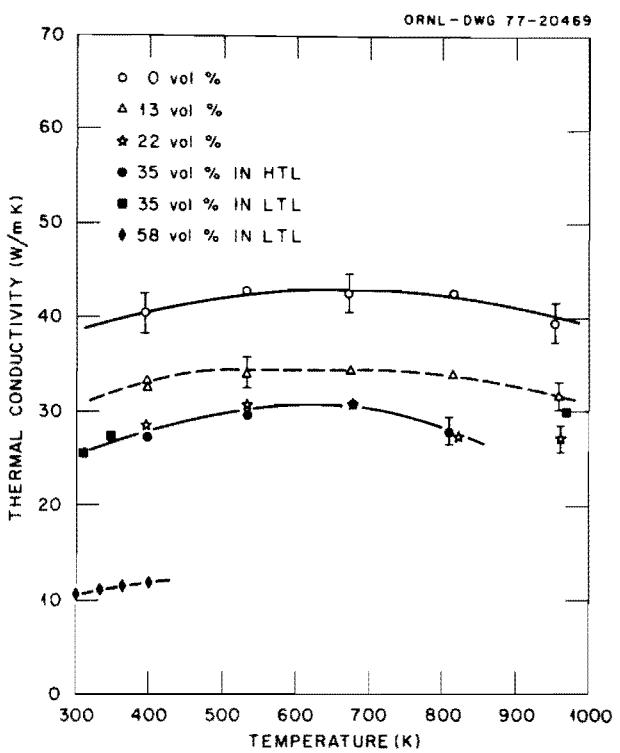

Fig. 16. Thermal conductivity of extruded and slug-injected fuel rods after one cycle in HFIR (~2×10^{25} neutrons/m^2) showing the low λ of the specimen containing 58-vol % particles and the λ agreement of the 23- and 35-vol % specimens.

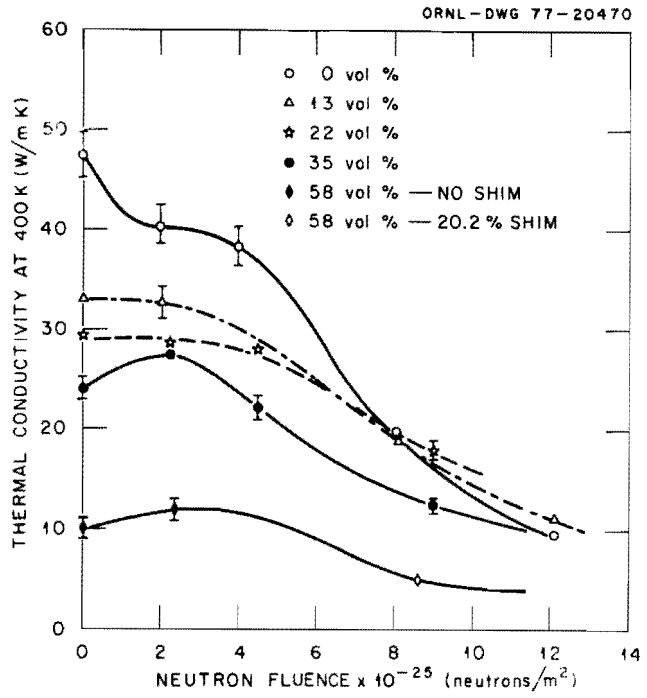

Fig. 17. The λ at 400 K vs fluence showing the initial increases in λ of the extruded specimen with 35-vol % particle and the slug-injected specimen. The high fluence decrease in λ of all specimens is also shown.

DISCUSSION OF RESULTS

The materials studied in this work were complex-multiphase solids. Even the simplest extruded specimen with 0-vol % particles consisted of anisotropic graphite flake, carbonaceous pitch between the flakes, and pores of all shapes. Specimens containing simulated fuel particles were the most complex because each particle consisted of three distinct phases. Thus, most specimens consisted of six distinct phases and the effects of these on the λ, ρ, S, and CTE were difficult to access because neutron fluence, irradiation temperature, and measurement temperature usually have different effects on each phase. Generally, a total property change is the sum of several mechanisms acting on different phases; these mechanisms sometimes compete and sometimes augment each other. Therefore, in this discussion we present some possible explanations and indicate the problem areas with the analysis.

Coefficient of Thermal Expansion

The CTE results at 298 and 973 K indicate that complex stress states occur in the extruded specimens and are quite different for the pure matrix sample and for those containing coated particles. It should be remembered that these samples were heat treated at 2100 K during fabrication, were irradiated at a nominal 1220 K, and were measured to only 973 K. One may reasonably assume that the specimens were essentially stress free at 2100 K, but on cooling to room temperature, interaction between the matrix (unirradiated CTE of $\sim 2 \times 10^{-6} \cdot K^{-1}$) and the particles (unirradiated CTE of $\sim 3.75 \times 10^{-6} \cdot K^{-1}$) would cause significant stress. The observed linear relation of CTE to particle loading for the unirradiated samples at 298 and at 973 K is a strong indication that microcracks are

not significant factors. This implies that, at least for the extruded specimens, residual stress must increase with particle loading but does not exceed the strength of the body.

After neutron irradiation, the thermal expansion characteristics are changed markedly as shown in Fig. 12 and are still quite different for the pure matrix and for the samples that contain particles. At 298 K, the 0-vol % particle sample had the lowest CTE after one HFIR cycle, and then the CTE increased with fluence, approaching the unirradiated value. The particle-containing samples experienced a similar decrease in CTE at 298 K after the first HFIR cycle, but the CTE continued to decrease with increasing fluence. This is most pronounced for the 22-vol % sample, but much less so for the 13 vol %. It is unfortunate that four- and six-cycle data could not be obtained for the 35% samples, but the one- and two-cycle results are essentially the same as for the 22% samples. At 973 K, the 0-vol % samples had CTEs almost independent of fluence and equal to the unirradiated sample. The loaded samples showed the same trends at the high temperature as at 298 K with a decrease in CTE with fluence, but the change is somewhat less for higher fluences.

These results suggest that at least two different mechanisms are affecting the expansion behavior of these samples after neutron irradiation. First, the measured volume decrease on irradiation (Fig. 11) and the corresponding decrease in CTE at 298 K coupled with the very small change in CTE at 973 K is indicative of extensive microcracking caused by unequal irradiation-induced shrinkages of the graphite filler flakes and the carbonaceous binder in the 0%-loading samples. Further neutron irradiation results in a volume increase which tends to close these microcracks in the matrix material so they have a decreasing effect on CTE. Second, the similar volume changes in the particle-containing samples, but the completely opposite CTE changes with increasing fluence, suggest a strong particle-matrix interaction. A possible mechanism would be a densification of the outer layer of the microsphere and graphitization-densification of the adjacent matrix material. This would result in a net tensile stress throughout the matrix and a corresponding decrease in CTE at both the low and high temperatures. This second mechanism would tend to be tempered by microcracks as suggested by the general coalescence of the results at 973 K, but the net tensile stresses still dominate.

Transport Properties

The thermal conductivity (λ) behavior of the simulated fuel rods is rather complex because there are many components including carbon core, pyrolytic carbon coatings, filler flake, and carbonaceous material between filler flakes and particles. Within each solid component there are three possible conduction mechanisms, so the total λ is given by

$$\lambda = \lambda_v + \lambda_e + \lambda_r \,, \tag{1}$$

λ_v = component due to quantized lattice vibrations,

λ_e = electronic component,

λ_r = radiation component.

In all solids within these fuel elements, λ_e and λ_r are negligible, so heat conduction is due to quantized lattice vibrations or phonons. The value of λ_v could definitely differ in each component. In addition to the conduction through various solid components, some heat possibly could be conducted across pores by radiation or gaseous conduction. Although both of these are negligibly small, pores still have an effect on λ. Spheroidal pores have relatively small effects on λ compared to the effect of flat

or open pores aligned so that the normal to the pore plane is parallel to the heat-flow direction. The behavior of ρ often provides an indication of how λ will behave.

The plateaus in the ρ curves (Fig. 13) between 3×10^{25} and 5×10^{25} neutrons/m^2 and the increase in λ of the specimens containing 22-, 35-, and 58-vol % particles are two of the most interesting features of the data. The relationship of these two properties presents a possible reason for the λ behavior. Figure 18 shows a solid curve[21] for the thermal conductivity versus the electrical conductivity, $\sigma = \rho^{-1}$, which passes within $\pm 10\%$ of most data on dense, isotropic, and unirradiated graphites. As graphites of this type are irradiated with neutrons, the values move away from the curve as noted by results on AXM-5Q and H-337 graphite.[3] This reduction in λ is caused by carbon atoms being disordered within or removed from the basal planes of the graphite particles within the isotropic solid. This disordering by neutrons actually moves the graphite material back toward a carbonaceous state similar to its condition prior to graphitization by heating to temperatures of 2800 to 3000 K.

However, several components of the simulated fuel rods in this investigation were poorly graphitized because the highest temperature employed during fabrication was only 2100 K. This poor graphitization of at least one important component within the fuel rod causes the λ:σ values to fall significantly below the curve for graphite. The λ:σ relation is nearly linear with data scatter within $\pm 7\%$. After one irradiation cycle ($\sim 2 \times 10^{25}$ neutrons/m^2), the results from the simulated fuel rods move closer to the curve for graphite. With additional irradiation the λ:σ values begin to decrease, but this is not shown in the figure. This behavior indicates that neutron irradiation at the high irradiation temperatures[4] ($\sim$1223 K) caused increased lattice order within all specimens including those fabricated by slug injection. Previous investigators[4] have ascribed this increase to ordering of the carbonaceous material immediately adjacent to the graphite filler flakes due to high-temperature neutron irradiation.

The fuel rods are complex composite systems with regard to energy transport, and it is difficult to state categorically the functions of each component in the total property behavior. There are, however, several possibilities including the following.

1. The thermal conductivity, λ_m, of the matrix material surrounding the fuel particles is the same (with the exception of a slight shift for minor density variation) as the thermal conductivity of the extruded specimen with no particles present. In this case the effective particle thermal conductivity, λ_p, would be free to move as needed to give the net λ.

2. The λ_p remains constant with fluence and λ_m would have a different behavior than does λ of the 0-vol % element.

3. A combination of the above two.

The first possibility is examined in Appendix B based on composite studies by others.[22,23] The results, which are shown in Fig. 19, would indicate that λ_p increases during the first cycle, decreases during the second, and then increases rapidly up to the maximum fluence of 12.1×10^{25} neutrons/m^2. The λ_p of 50 W/m·K after 12.1×10^{25} neutrons/m^2 appears unreasonably large, but values over 400 W/m·K have been measured along the basal planes of pyrolytic carbon with a density of 2.1 Mg/m^3

21. D. L. McElroy, T. G. Kollie, W. M. Ewing, R. S. Graves, and R. M. Steele, *Room Temperature Measurements of Electrical Resistivity and Thermal Conductivity of Various Graphites*, ORNL TM-3477 (1971).

22. J. M. Wimmer, H. C. Graham, and N. M. Tallan, "Microstructural and Polyphase Effects," chap. 9 in *Electrical Conductivity in Ceramics and Glass, Part B*, N. M. Tallan, Ed., Marcel Dekker, Inc., N.Y., 1974.

23. A. Eucken, Forsch. Gebiete Ingenieurw. B 3, Forschungsheft No. 353, 16 pp., 1932; *Ceram. Abstr.* 11(11), 576 (1976); *Ceram. Abstr.* 12(6), 231 (1933).

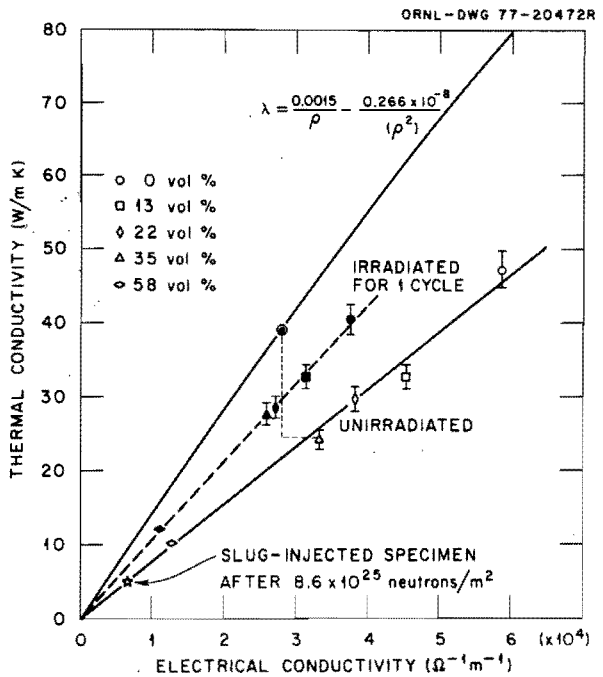

Fig. 18. The λ vs σ (ρ^{-1}) of the simulated fuel rods prior to irradiation and after one cycle in HFIR. A comparison line for isotropic graphites is also shown. The circled value near the solid line was obtained on the unirradiated 35-vol% specimen after heating to 2900 K for 1.8 ks.

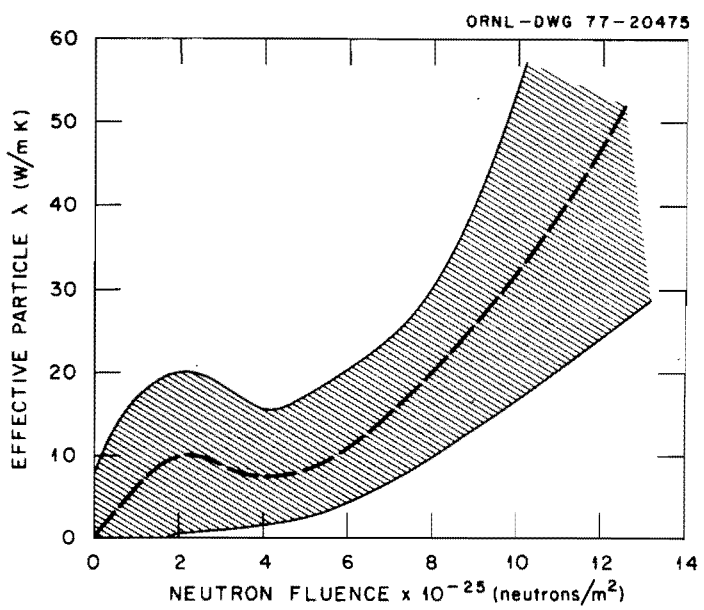

Fig. 19. Effective particle thermal conductivity, λ_p, showing the increase with increasing neutron fluence calculated on this model.

(ref. 24), (as compared to the 2 Mg/m^3 in the present case). The basal (high thermal conductivity direction) planes are aligned in such a manner that they have the maximum effect in conducting heat around the particle and hence a maximum effect on λ of the simulated fuel rods. Pyrolytic carbons that were irradiated in the same capsules employed for this study[25] showed that the anisotropy, as determined by BAF measurements, increased with neutron fluence and, further, that the anisotropy increase was much greater when the pyrolytic carbon was constrained during neutron irradiation. Thermal expansion differences within the simulated fuel rods of this study would have caused strain on the outer coatings of the particles. Therefore, some increase in λ_p would not be surprising since the combination of neutron flux and mechanical stress on the outer pyrolytic carbon could have caused sufficient strain to improve the basal plane alignment around the particle surface. Quantitative calculations on this would be difficult—if not impossible— because the ordering is sensitive to many parameters including coating deposition rate and mechanical strain.

The second possibility for explaining the λ and ρ results involves the assumption that λ_m between the particles of extruded elements does not behave as does the element that contains no particles. Other investigators have shown that neutron flux on a carbonaceous material at high temperature causes a partial ordering around the small graphite filler flakes.[4] This partial ordering can cause a net increase in λ, although λ of the filler flakes begins to decrease with the inception of neutron flux. This effect is seen in Fig. 16, which shows a distinct inflection of λ versus fluence for the specimen with 0-vol % particle loading. This partial ordering around filler flakes is increased when the carbonaceous material is strained by the presence of particles. Thus, the specimens with the most particles would be expected to show the greatest effect as was observed in this case; the 35- and 58-vol % specimens have the greatest percentage of λ increase.

The most likely explanation is that the transport properties results were controlled by a combination of the above two factors. That is, the initial increases in λ of the 35-vol % extruded and 58-vol % slug-injected simulated fuel rods and the curvatures of the λ versus fluence curves of the 13- and 22-vol % specimens are due to an unknown combination of ordering within the outer particle coating and within carbonaceous material adjacent to filler flakes. The latter effect caused the inflection in the λ versus fluence curve for the extruded specimen with no particles present.

If this general interpretation is correct, heat treatment of some simulated fuel elements to temperatures normally employed for graphitization should change the properties in a manner analogous to the first irradiation cycle. This was tested by heat treating the unirradiated extruded specimen with 35-vol % particles to 2900 K for 1.8 ks. This treatment increased the ρ from 30 $\mu\Omega\cdot m$ to 35.6 $\mu\Omega\cdot m$, which is similar to the initial irradiation cycle increase to 38.7 $\mu\Omega\cdot m$. The λ at 400 K increased from 24.4 $W/m\cdot K$ to 39.0 $W/m\cdot K$, which is also similar to the λ increase during the first cycle of neutron irradiation. This result is shown in Fig. 18. Graphitization at 2900 K also increased the absolute Seebeck coefficient in the same way as the initial neutron irradiation. This behavior of these three properties tends to substantiate the interpretation of partial graphitization occurring in some important conduction phase (probably the carbonaceous material within the matrix) during the first irradiation cycle.

24. Y. S. Touloukian, Ed., "Elements," p. 89 in *Thermophysical Properties of High Temperature Solid Materials*, vol. 1, Purdue Research Foundation, 1967.

25. J. E. Kaae, R. E. Bullock, C. B. Scott, and D. P. Harmon, *The Mechanical Behavior of BISO Coated Fuel Particles During Irradiation, Parts I and II*, GA-A14052 (July 1976).

Wagner[26] has investigated the effects of final heat-treatment temperatures on graphite flour bonded with polyfurfuryl alcohol and graphite flour bonded with pitch. The λ values that he obtained are within 12% of the present value for unirradiated material with 0-vol % loading after corrections are made to a common density. This agreement is excellent when one considers the errors involved with experimental measurements and vagaries of fabrication. Wagner's results show that the thermal conductivity of the 0-vol % specimen probably could be increased about 60% by increasing the final fuel element heat-treatment temperature from 2100 to 2800 K. At 400 K the λ increase in the above specimen was 59.8%. Although this increased λ from the higher heat treatment possibly would be short lived under neutron irradiation, it would significantly reduce the gradient across the fuel particles in the initial stages of reactor operation.

The explanation of the CTE results was based on microcracks appearing in the matrix material during irradiation. These microcracks, if present, would negate part of the possible λ increase around the filler flakes. As mentioned earlier, however, the various properties are related to many variables in different ways so that the explanations of both CTE and the transport properties are qualitatively correct.

As an addendum to this work, the ρ of production fuel elements containing ThO_2 particles was measured versus shim loading. These results, which are described in Appendix C, show that ρ decreases with increasing shim content, but even a high shim loading does not eliminate the effect of the low-density slug-injection matrices in increasing ρ.

CONCLUSIONS

1. The λ of simulated extruded fuel rods was a factor of 2 to 4 greater than the λ of slug-injected fuel rods depending on the comparison temperature and neutron fluence. The λ of the unloaded extruded specimens (0 vol %) decreases with increasing neutron fluence, whereas λ of the specimens with high loading tends to increase initially and then decrease at high neutron fluence.

2. The ρ of each loading increases with neutron fluence. However, the ρ of the extruded specimens tends to plateau over a wide fluence range followed by a rapid increase at high fluence, whereas the ρ of slug-injected specimens appears to increase continually with fluence.

3. After a neutron fluence of 8.6×10^{25} neutrons/m^2, a slug-injected simulated fuel rod has a λ of 5 W/m·K, which is about 30% below the HTGR design value of 6.9 W/m·K.

4. Analysis of the ρ and λ data suggests that a partial ordering occurs in the fuel rods during neutron irradiation at 1223 K. This concept is supported by the behavior of a 35-vol % specimen when heat treated to 2900 K. Therefore, some ordering may be occurring around the graphite filler flakes in the carbonaceous matrix, and this ordering tends to increase the fuel element λ. This increase is being countered by decreases in λ of the filler flakes as well as possible microcracking. Assumption that the matrix material between the particles of extruded fuel rods has the same λ as the unloaded extruded fuel rod leads to a calculated effective particle λ that increases to unreasonably high values.

5. Prior to irradiation the CTE of each specimen increases smoothly with temperature, and CTE at any temperature increases smoothly with increasing particle loading.

6. After irradiation the CTEs of these materials are no longer strongly dependent on volume percent particle loading or neutron fluence, and temperature has a reduced effect.

26. P. Wagner, *Effect of Heat Treatment Temperature on Binder Thermal Conductivities*, LA-6181 (February 1976).

7. The CTE and volume change data suggest that extensive microcracking may be occurring in the carbonaceous binder between filler flakes and that the particles and matrices are bonded strongly, which causes tensile stress throughout the matrices.

RECOMMENDATIONS

1. Irradiation temperatures other than the one used in this experiment could make λ differ from these results. Thus, caution should be exercised in application of the data.

2. The macroscopic λ of the slug-injected fuel rods should not be used for calculation of temperature gradients across fuel particles because the matrix of slug-injected rods can be so porous that many particles are almost surrounded by gas. Hence, across any particle the gradient could be greater or less than calculated.

3. Properties of slug-injected material with inert particles should be determined versus shim loading and type, irradiation temperature, and neutron fluence. The λ of unirradiated slug-injected fuel rods containing actual fuel particles should be determined versus shim concentration.

4. Detailed ceramography of all specimens in this study should be done to verify the conclusions drawn with regard to the behavior of carbonaceous material between filler flake during neutron irradiation.

5. Routine ρ measurements might be useful to determine the homogeneity of actual fuel rods. Although these measurements would have to be made on unfired fuel elements, large defects such as cracks should be detectable.

ACKNOWLEDGMENTS

The authors are grateful to D. E. Rosson, R. L. Hamner, and J M Robbins for sample fabrication and also to the latter for answering numerous questions. We also thank P. Angelini for obtaining some production specimens and R. L. Beatty and D. L. McElroy for constructive comments on the test. We also take this opportunity to express our gratitude to Sharon Buhl for her patience in the draft preparation. The report was edited and prepared for reproduction by the Technical Publications Department.

Appendix A

EXPERIMENTAL DATA

Measured values of ρ, S, and λ for the simulated fuel rods involved in this study are given in Tables A-1 through A-6. In addition to the tabulated ρ results for each specimen, ρ values obtained near 300 K on a knife edge are given in Tables 1 and 6 of the main text.

An archive slug-injected specimen with 36.5-vol % simulated fuel particles and 20.2-vol % shim produced a λ of 4.9 W/m·K at 294.2 K and 5.2 W/m·K at 350.6 K after 8.6×10^{25} neutrons/m^2 ($E > 28.8$ fJ).

Table A-1. Measured values of ρ, S, and λ of extruded specimens with 0-vol % particle loading

Temperature (K)	λ (W/m·K)	S (μV/K)	ρ ($\mu\Omega$·m)
	Unirradiated		
393.9	47.5	5.8	
538.1	45.1	5.3	14.8
673.0	43.7	4.6	14.1
815.7	43.0	4.3	13.6
952.8	38.6	4.8	13.2
952.8	35.6	4.8	
533.9	48.0	5.3	
	2.02×10^{25} neutrons/m^2 1 cycle in HFIR		
393.0			24.2
397.2	40.5	10.1	
532.5	42.8	9.8	21.3
672.3	42.6	8.6	19.0
806.4	43.0	7.5	17.5
953.9	39.4	6.7	16.1
	4.03×10^{25} neutrons/m^2 2 cycles in HFIR		
392.8	38.4	12.2	28.8
534.8	39.4	12.2	26.1
675.6	38.0	11.1	22.9
813.5	36.9	9.7	20.4
952.6		8.5	18.4
392.8	38.8	11.1	26.1
	8.05×10^{25} neutrons/m^2 4 cycles in HFIR		
394.9	20.0	15.4	36.5
531.3	21.7	17.6	32.8
671.4	21.7	18.4	29.7
809.3	21.8	17.5	27.1
955.1		16.2	24.9
531.2	21.9	15.6	33.2
	12.1×10^{25} neutrons/m^2 6 cycles in HFIR		
393.8	9.3	13.6	63.4
532.9	10.5	16.6	58.4
674.4	11.1	18.4	53.7
809.9	11.4	18.8	49.8
955.2	11.4	18.8	46.0
533.6	10.5	15.9	59.0

Table A-2. Measured values of ρ, S, and λ of extruded material with 13-vol % particle loading

Temperature (K)	λ (W/m·K)	S (V/K)	ρ ($\mu\Omega\cdot$m)
	Unirradiated[a]		
393.4	32.8	9.7	*a*
532.0	35.0	7.6	*a*
667.9	35.1	6.0	*a*
805.6	34.2	1.1	*a*
950.4	31.5	3.6	*a*
533.2	34.8	5.8	*a*
	2.02×10^{25} neutrons/m^2 1 cycle in HFIR		
397.8	32.5	12.8	
396.6	33.3	13.4	29.2
532.3	34.1	13.6	25.8
672.9	34.3	12.0	23.2
813.5	34.0	10.5	21.2
948.0	31.7	9.7	19.7
	4.03×10^{25} neutrons/m^2 2 cycles in HFIR		
392.3	29.5	16.9	31.7
531.3	30.2	17.5	28.1
676.7	30.0	16.6	25.0
813.0	29.2	14.9	22.8
954.1	29.0	12.9	20.7
393.1	28.8	15.8	31.7
	8.05×10^{25} neutrons/m^2 4 cycles in HFIR		
393.7	18.7	15.9	40.62
532.5	20.3	18.3	36.56
673.2	20.9	19.1	33.06
814.0	20.8	18.2	30.11
956.2	20.7	16.7	27.47
392.9	19.1	14.8	40.41
	12.09×10^{25} neutrons/m^2 6 cycles in HFIR		
394.2	11.4	15.5	62.0
534.3	12.4	17.8	55.7
673.7	12.6	18.4	50.4
813.4	12.5	17.6	45.9
955.2			41.9
538.3	12.2	16.4	55.4

[a]Lost current lead which prevented ρ measurements.

Table A-3. Measured values of ρ, S, and λ of extruded simulated fuel rods containing 22-vol % particle loading

Temperature (K)	λ (W/m·K)	S (μV/K)	ρ ($\mu\Omega$·m)
	Unirradiated		
392.7	29.5	7.5	24.9
530.0	30.3	8.1	23.2
671.9	30.6	8.2	22.0
807.1	29.9	8.4	21.2
681.6	30.3	6.9	22.0
956.4	30.2	9.3	20.4
397.1	28.6	13.2	33.5
535.0	30.7	12.9	29.4
677.1	31.0	11.5	26.2
814.5	27.9	9.9	23.9
960.2	27.2	8.9	22.0
	2.26×10^{25} neutrons/m^2 1 cycle in HFIR		
393.2	28.0	14.5	36.1
533.8	28.9	14.7	31.7
672.9	28.5	13.7	28.2
812.8	27.8	12.0	25.4
954.3	27.0	10.7	23.1
534.2	28.9	14.0	31.5
	4.5×10^{25} neutrons/m^2 2 cycles in HFIR		
393.4	18.0	13.9	47.2
533.6	19.2	15.2	42.0
673.4	19.3	15.0	37.6
813.8	18.7	13.9	33.9
953.0	18.4	12.8	30.9
533.9	19.1	14.3	41.9
	6 cycles in HFIR		
	Broken		

Table A-4. Measured values of λ, ρ, and S of extruded simulated fuel rods containing 35-vol % particle loading

Temperature (K)	λ (W/m·K)	S (μV/K)	ρ (μΩ·m)
	Unirradiated		
395.9	24.4	8.3	28.4
536.9	24.6	9.5	26.6
671.8	24.2	10.3	25.3
823.9	22.0	11.2	24.3
953.6			23.9
	1 cycle in HFIR		
394.6	27.5	14.9	35.3
534.5	29.9	15.0	31.2
672.7	31.0	13.9	28.0
811.3	27.9	12.1	25.4
952.6	30.0	11.3	22.9
	Check of 1 cycle specimen in low-temperature longitudinal		
309.7	26.1		
308.7	25.6 in argon		
348.1	27.7		
	4.5×10^{25} neutrons/m^2 2 cycles in HFIR		
399	22.4	17.2	36.6
534	25.0	18.0	32.5
673	27.3	17.1	29.1
812	27.9	15.5	26.5
955	29.9	14.7	24.0
	9.0×10^{25} neutrons/m^2 4 cycles in HFIR		
423	12.9	16.3	46.2
576	13.4	17.9	40.9
723	14.7	17.9	36.6
874	13.4	16.6	33.1
	6 cycles in HFIR		
	Broken		

Table A-5. Measured transport properties of an unirradiated 35-vol % extruded specimen after heat treatment to 2900 K for 1.8 ks

Temperature (K)	λ (W/m·K)	S (μV/K)	ρ (μΩ·m)
295.0			35.6
394.1	39.4	9.71	
473.6	38.0	8.78	
574.0	35.8	7.29	

Table A-6. Measured physical properties of several slug-injected specimens with 58-vol % particle loading

Temperature (K)	λ (W/m·K)	S (μV/K)	ρ (μΩ·m)
	Unirradiated		
393.9	9.9	10.1	74.0
532.5	10.3	12.8	68.9
675.8	12.2	14.8	63.5
813.7	9.8	16.4	60.5
963.6	10.5	18.0	55.9
394.7	10.4	9.9	71.6
	1 cycle		
298.4	10.7	19.3	
332.7	11.2	20.4	
363.8	11.5	20.5	
400.7	11.8	20.8	

Appendix B

CALCULATION OF AN EFFECTIVE PARTICLE λ ASSUMING THAT λ_{matrix} BEHAVES AS DOES λOF THE UNLOADED SPECIMEN

Many attempts have been made to mathematically relate the component λ values to λ of the composite, and some of these attempts are discussed elsewhere.[22] The most frequently employed equation[22] is

$$\lambda/\lambda_m = \frac{1 - 2p(\lambda_m - \lambda_p)/(2\lambda_m + \lambda_p)}{1 + p(\lambda_m - \lambda_p)/(2\lambda_m + \lambda_p)}, \tag{B-1}$$

where

λ = thermal conductivity of composite,

λ_m = thermal conductivity of the continuous phase,

λ_p = thermal conductivity of the discontinuous phase,

p = volume fraction of discontinuous phase.

This equation was derived for composites with discontinuous-spheroidal particles separated sufficiently that the thermal field becomes uniform between adjacent particles. The latter restricts use of the equation to values of p less than 0.15.

This experiment was planned with the hope that the matrices of all loadings would have the same density—and hence the same conductivity—as the material with 0-vol % particles. As Table 1 shows, however, this condition was not met, and the above equation was first used to calculate the matrix

conductivity for each loading by treating additional porosity as spherical voids with a $\lambda_p' \equiv 0$. For this case the above equation reduces to

$$\lambda' = \lambda_1' \frac{1 - p'}{1 + 0.5\,p'} \quad , \tag{B-2}$$

where

λ_1' = thermal conductivity of the 0-vol % specimen,

λ' = thermal conductivity of the matrix material with additional porosity p'.

Thus, the specimen with 35-vol % particles at 400 K was assumed to have a matrix conductivity of

$$\lambda' = 47.5 \frac{1 - 0.0857}{1 + 0.0429} = 47.5(0.875) = 41.6 \text{ W/m·K} , \tag{B-3}$$

since

$$p' = \frac{1.75 \text{ Mg/m}^3 - 1.60 \text{ Mg/m}^3}{1.75 \text{ Mg/m}^3}$$

and $\lambda_m' = 47.5$ W/m·K at 400 K from Table 5. This approach yielded λ_m values of 41.6, 44, and 46 W/m·K for the matrices of the composite fuel elements with loadings of 35-, 22-, and 13-vol % respectively.

Equation B-1 was then used to calculate values of λ/λ_m at specific values of 0.13-, 0.22-, and 0.35-vol fraction particles for assumed values of 0, 10, and 20 W/m·K for the thermal conductivity of the second phase simulated fuel particles. The results of these calculations are shown in Fig. B-1. Smooth curves were drawn between the three discrete data for each assumed value of λ_2. This "theoretical calculation" can be compared to the experimental results at each irradiation stage as shown. Although the "experimental value"* for λ/λ_m for the 13-vol % unirradiated specimen appears distressingly low, assumed λ_p values near zero for unirradiated material and between 5 and 10 W/m·K after one cycle would fit the experimental data well. This result indicates that λ of the simulated fuel particle increases with initial fluence.

The relatively large deviation of λ/λ_m from the experimental data on 35-vol % particle loading after 1 cycle is not significant because the equation is in error at that high loading. Figure B-1 shows results which would indicate that λ_p increases during the first cycle, decreases during the second, and then increases rapidly up to the maximum fluence of 12.1×10^{25} neutrons/m^2. This behavior is shown in Fig. 19 of the text.

*The "experimental value" now has an obvious hedge since we made an estimate of the matrix thermal conductivities using Eq. B-3 and 47.5 W/m·K for the unirradiated specimen of 0-vol % loading.

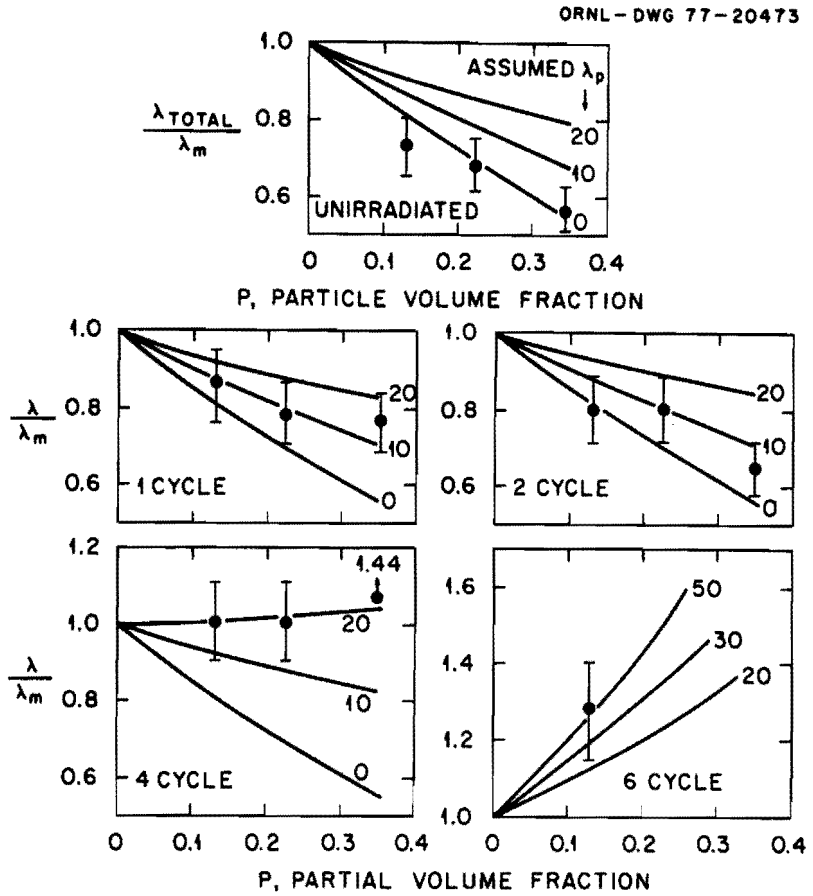

Fig. B-1. Effective particle thermal conductivity, λ_p, showing the increase with increasing neutron fluence. This was obtained on a model which assumed that the matrix λ was similar to that of the extruded 0-vol % rod. A calculated set of curves is shown for each irradiation stage, and measured values are shown for comparison.

Appendix C

COMPARISON OF THE ELECTRICAL RESISTIVITIES OF SLUG-INJECTED RODS CONTAINING FUEL PARTICLES TO RODS CONTAINING SIMULATED PARTICLES AND TO EXTRUDED RODS

The ρ of several production specimens containing ThO_2 fuel kernels was measured for comparison to the research specimens that contained inert carbon kernels. The results are given in Fig. C-1, which shows ρ (300 K) versus volume percent shim content. The ρ of this material with 0 shim is greater than that of the research specimen formed with slug injection by 20%. The two sets of production materials with 36% fuel differed by nearly 20%. The extruded rods are also shown in the figure in terms of "equivalent" shim content. The great difference in the two curves merely suggests in another way that λ of the extruded material should be much higher than λ of the slug-injected material. This is true regardless of shim content although λ probably increases slightly with increasing shim content.

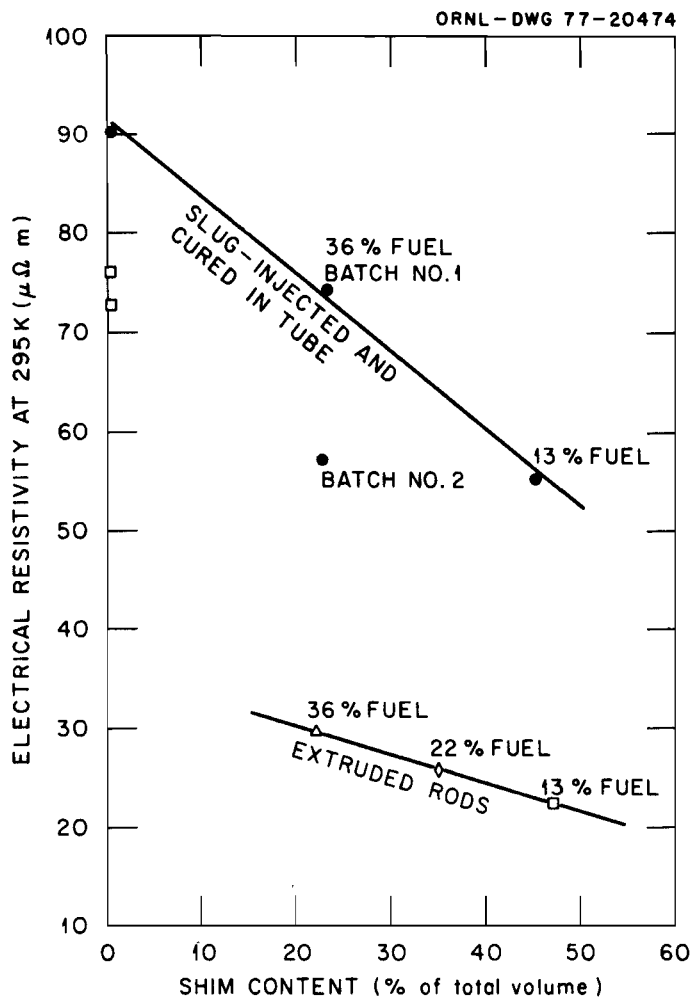

Fig. C-1. Electrical resistivity vs shim content for slug-injected fuel rods and vs "equivalent" shim content for extruded fuel rods. This shows that the ρ of slug-injected elements with shim added is about two times greater than extruded fuel rods.

ORNL-5414
Distribution Category UC-77

INTERNAL DISTRIBUTION

1–2. Central Research Library
3. Document Reference Section
4–5. Laboratory Records Department
6. Laboratory Records, ORNL
7. ORNL Patent Office
8. E. J. Allen
9. R. L. Beatty
10. B. J. Bolfing
11. R. A. Bradley
12. R. J. Braatz
13. A. J. Caputo
14. B. F. Crump
15. B. C. Duggins
16. W. P. Eatherly
17–21. T. G. Godfrey
22. R. J. Gray
23. R. S. Graves
24. J. L. Heck
25. L. C. Henley
26. R. F. Hibbs
27–29. M. R. Hill
30. F. J. Homan
31. D. R. Johnson
32. M. J. Kania
33–42. P. R. Kasten
43. J. J. Kurtz
44. W. J. Lackey
45. Eal H. Lee
46. C. T. Liu
47–49. E. L. Long, Jr.
50. J. E. Mack
51. D. L. McElroy
52–57. J. P. Moore
58. J. W. Moore
59. K. J. Notz
60. A. R. Olsen
61. H. Postma
62. T. C. Reiley
63. J. E. Selle
64. T. N. Tiegs
65. D. B. Trauger
66. F. J. Weaver
67. G. C. Wei
68. R. G. Wymer
69. R. W. Balluffi (consultant)
70. P. M. Brister (consultant)
71. W. R. Hibbard, Jr. (consultant)
72. N. E. Promisel

EXTERNAL DISTRIBUTION

73–74. DOE DIVISION OF NUCLEAR POWER DEVELOPMENT, Washington, DC 20545
Director
Assistant Director, HTGR Development
75. SAN-DEVELOPMENT, SAN DIEGO AREA OFFICE, P.O. Box 81325, San Diego, CA 92138
Senior Program Coordinator
76–78. DOE OAK RIDGE OPERATIONS DIVISION, P.O. Box E, Oak Ridge, TN 37830
Director, Research and Technical Support Division
Director, Reactor Division
H. W. Behrman, Reactor Division
79–255. DOE TECHNICAL INFORMATION CENTER, P.O. Box 62, Oak Ridge, TN 37830
For distribution as shown in TID-4500 Distribution Category, UC-77 (Gas-Cooled Reactor Technology)

☆U.S. GOVERNMENT PRINTING OFFICE: 1978-740-190/140